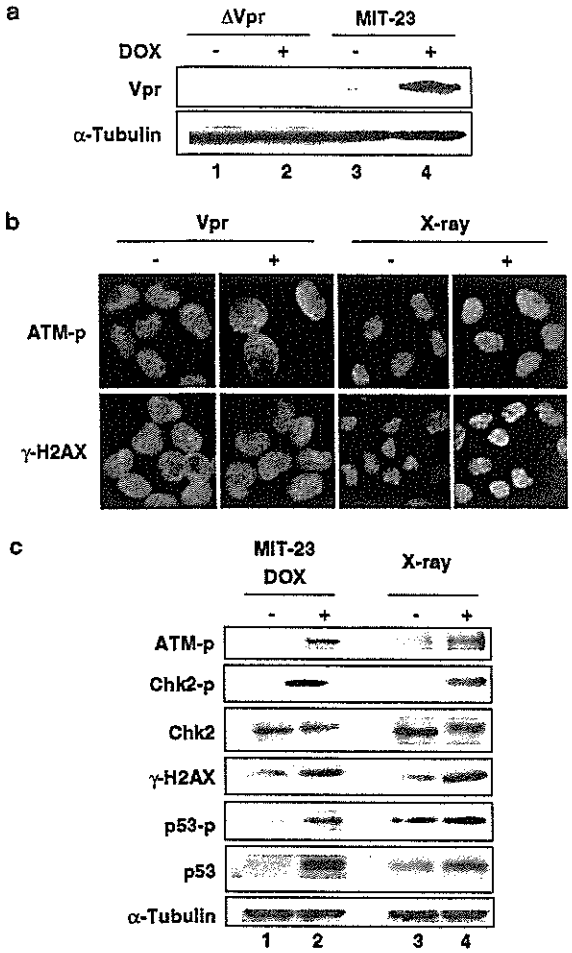

Figure 2 Activation of DSB-induced cellular signaling. (**a**) Expression profiles of Vpr in MIT-23 cells. Vpr expression was induced in 48 h with 3 μg/ml DOX in MIT-23 cells. The Vpr expression level in MIT-23 cells was analysed by Western blotting with the Vpr-specific antibody 8D1. (**b**) Focus formation of phosphorylation of ATM (ATM-p) and γ-H2AX following Vpr expression. The cells were stained with specific antibodies against ATM-p and γ-H2AX. The signals for ATM-p and γ-H2AX are depicted as red spots in the nucleus (blue). (**c**) Western blot analysis of proteins involved in the DSB-induced signal pathway. Cell lysates of MIT-23 cells (lanes 1 and 2) were subjected to analysis. As a positive control, HT1080 cells were irradiated at 7.5 Gy, collected after 30 min, and subjected to analysis.

ATM-p or γ-H2AX in DOX-treated ΔVpr cells, in which only the *vpr* gene was eliminated from vectors that were utilized for the establishment of MIT-23 cells (data not shown). Western blot analysis also detected that DNA-damage-sensing signals were induced by Vpr expression (Figure 2c). Interestingly, Chk2, a substrate of ATM, was highly phosphorylated at threonine 68 by Vpr expression (Figure 2c, lane 2). Additionally, p53 expression as well as its phosphorylation also increased as a downstream response of these molecules. Consistent with the previous report showing that Chk1, a substrate of ATR, is activated by Vpr (Roshal *et al*., 2003), we observed the presence of the slowly migrating band of Chk1 as its phosphorylated form under Vpr expression (data not shown).

To compare the Vpr-induced DSB-dependent signals with those by X-ray irradiation, HT1080 cells were irradiated with 7.5 Gy of X-rays, and the evoked signals were analysed. As shown in Figure 2b (right panels), X-ray-induced DSBs generated focus formation of ATM-p (Figure 2b, upper panel) and γ-H2AX (lower panel). Additionally, Western blot analysis clearly demonstrated the phosphorylation of both Chk2 and p53 (lane 3 and 4). Data suggest that Vpr-induced DNA-damage signals are quite similar to those triggered by a well-characterized DSB inducer.

Mobilization of cellular factors that are involved in repair of DSBs

To further characterize the molecules activated as a cellular response to Vpr-induced DSBs, we investigated BRCA1, RPA and Rad51 mobilized for repair of DSBs (West, 2003). As shown in Figure 3, the immunohistochemical analysis carried out under Vpr expression clearly detected focus formation of these molecules (Figure 3). In contrast, control cells did not show remarkable modification of these molecules. Again, X-ray irradiation also induced the same modification of the molecules (Figure 3, right panels).

It has been proposed that during the DSB repair process, Rad51 is released from a complex of p53 and becomes competent for HR (Linke *et al*., 2003; Bertrand *et al*., 2004). To address this possibility, we compared the physical association of Rad51 and p53 in the insoluble chromatin fraction before and after the induction of Vpr expression. The interaction of these molecules was eliminated following Vpr expression (Figure 4a, lanes 3 and 4; arrow). The level of the complex formation of p53 and Rad51 decreased by 35% compared to the control. This finding is reproducibly observed, implying the possibility that Vpr binds either Rad51 or p53 and ceases their interaction. We examined the direct interaction of Vpr and Rad51 by using recombinant proteins, but did not obtain positive results (data not shown). As it has been shown that Vpr does not interact with p53 (Sawaya *et al*., 1998), the mechanism of dissociation of p53 and Rad51 in Vpr-expressing cells remains to be clarified.

We also compared this molecular change with that induced by X-ray irradiation. HT1080 cells were irradiated, and the subsequent change of the interaction of Rad51 and p53 was examined. As observed in Figure 4a, the interaction between Rad51 and p53 in the insoluble chromatin fraction was also abolished (Figure 4b, compare lanes 3 and 4, arrow). Data suggest that Vpr modifies Rad51 in the same way as X-ray irradiation.

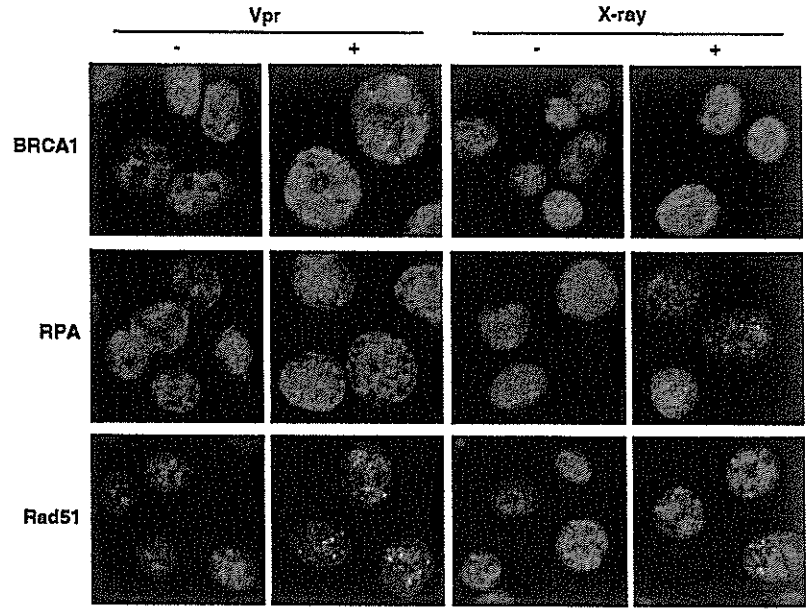

Figure 3 Involvement of BRCA1, RPA and Rad51 in Vpr-induced signaling. MIT-23 cells were cultured in the presence or absence of 3 μg/ml DOX for 48 h. Focus formations of BRCA1, RPA and Rad51 during Vpr expression are shown. These signals are visualized as red spots in the nucleus (blue).

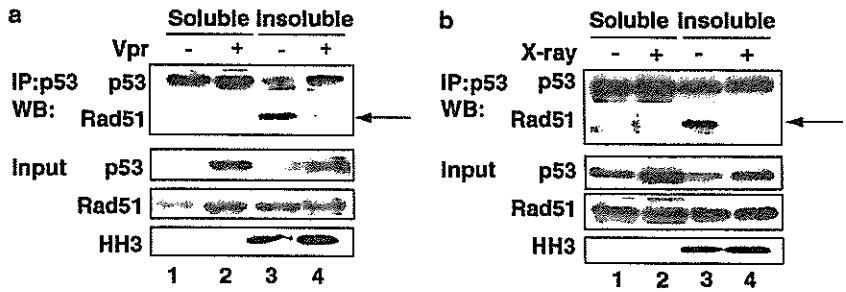

Figure 4 Dissociated interaction of p53 and Rad51 in a chromatin fraction during Vpr expression. The lysates of the soluble (lanes 1 and 2) and insoluble chromatin fractions (lanes 3 and 4) subjected to analysis. Proteins that were immunoprecipitated (IP) with the anti-p53 antibody (αp53) were analysed by Western blot analysis (WB) with the αp53 and αRad51 antibodies, respectively. Input lysates were also analysed by the same antibodies and αhistone H3 (HH3). The cell lysate with (lanes 2 and 4) or without (lanes 1 and 3) Vpr expression are shown (a). The same analysis was performed on X-ray irradiated cells (b). Arrowheads indicate Rad51 recovered by αp53 antibody.

Increased rate of HR by Vpr

DSBs must be correctly repaired, or genome integrity cannot be maintained (West, 2003). As Vpr induces DSBs and cellular factors such as Rad51 and BRAC1 are mobilized under Vpr expression, we hypothesized that the rate of HR increased in Vpr-expressing cells. To measure the rate of HR, we first utilized a system invented by Slebos and Taylor (2001) that could monitor extrachromosomal recombination within a plasmid DNA (pBHRF). pBHRF contains a truncated EBFP cassette, which forms a functional EGFP following intramolecular HR (Slebos and Taylor, 2001). We co-transfected HT1080 with pBHRF and a plasmid DNA encoding Vpr and examined the effects of Vpr on HR. After 72 h of transfection, the EGFP- and EBFP-positive cells were counted by flow cytometry (Figure 5a, regions a and b, respectively). Then, the frequency of HR was calculated as a ratio of number of cells positive for EGFP and EBFP. It increased about 2.5-fold by co-transfection of a plasmid encoding Vpr. Vpr-induced enhancement of HR was reproducibly observed ($P<0.05$), and the representative results are shown in Figure 5b.

Although the experiments with pBHRF strongly suggested that Vpr increases HR, it has been demonstrated that an extrachromosomal HR does not correlate with intrachromosomal HR. Waldman and Liskay (1987) clearly demonstrated that the frequency of

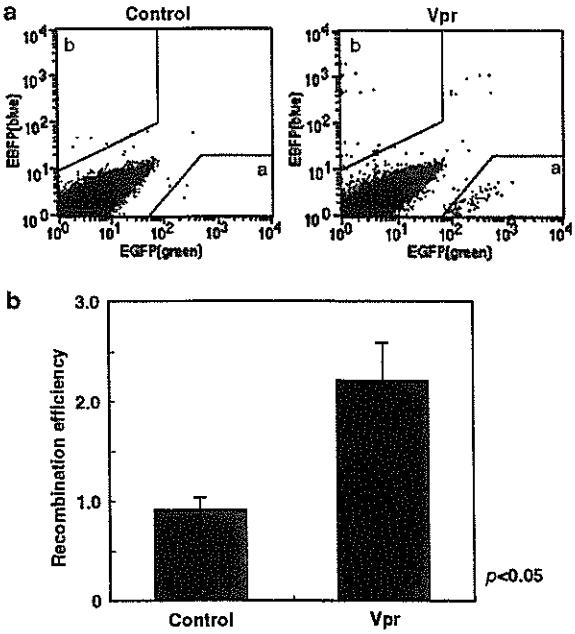

Figure 5 Increased rate of extrachromosomal HR by Vpr. (a) A representative result of three independent experiments with pBHRF. HT1080 cells were co-transfected with pBHRF and pcDNA3.1/Vpr (see Materials and methods section). The cells were subjected to analysis by flow cytometry after 72 h. Regions a and b were tentatively determined in a control sample. These indicate the areas where cells positive for EGFP (region a) or EBFP (region b) were not present in untreated samples. After treatment cell numbers in these areas were counted and compared. (b) Increase of GFP-positive cells by Vpr. The ratio of GFP-positive cells to BFP-positive cells, which are indicative of HR frequencies (Slebos and Taylor, 2001), were counted. Each sample was analysed twice in triplicate; bars ± s.d.

extrachromosomal and intrachromosomal recombination rates are differentially influenced by the mismatch of the nucleotides. To measure the rate of intrachromosoml HR under Vpr expression correctly, we prepared stable transfectants derived from HT1080 cells that had been introduced with pDR-GFP. pDR-GFP is a reporter construct that will generate an intact EGFP gene by gene conversion after digestion with a rare cutting enzyme, I-*Sce*I (Pierce *et al*., 1999). We obtained two independent transfectants, HT/DR-GFP-1 and -2, that possessed an integrated exogenous plasmid DNA competent for a short tract gene conversion (Supplementary information 1a) (Pierce *et al*., 1999). Then, HT/DR-GFP cells were infected with adenoviruses of either Adβgal or Ad-SceI-NG and subjected to analysis of GFP-positive cells after 72 h. After infection with Ad-SceI-NG, both clones gave increased numbers of GFP-positive cells (about 0.5%) (Supplementary information 1b and c). In contrast, Adβgal, control adenovirus, induced very few cells positive for GFP (<0.1%) (Supplementary information 1b and c).

We then examined the influence of Vpr on the rate of HR. First, we introduced a plasmid DNA encoding Vpr or its control plasmid DNA, but it was not possible to assess the effects of Vpr correctly because transfection of plasmid DNA by itself influenced the rate of HR (data not shown). It has been well reported that Vpr enters cells and expresses its biological activity when added to the cell culture (Jenkins *et al*., 1998; Henklein *et al*., 2000; Huang *et al*., 2000; Taguchi *et al*., 2004). These observations encouraged us to perform the experiments by adding Vpr to cells exogenously with subsequent measurement of GFP-positive cells. We prepared a recombinant Vpr (rVpr) (Hoshino *et al*., submitted), and we first checked whether exogenously added rVpr induces DSB-triggered cellular response. rVpr (50 ng/ml; 3.7 nM) added to the medium induced DSB-dependent signals (Figure 6a), whereas glutathione *S* transferase (GST), an irrelevant recombinant protein that was expressed in bacteria and purified, did not (right panels). Interestingly, the addition of the ATM inhibitor KU55937 abolished rVpr-induced focus formation of ATM-p and γ-H2AX (Figure 6a).

When rVpr was added to HT/DR-GFP-1 (clone-1), HR especially after infection with Ad-SceI-NG-infected was definitely enhanced (about 1.5%), whereas it was not remarkably changed by the addition of GST (Figure 6b and c, left panel). The difference in GFP-positive numbers after treatment with rVpr and GST was statistically significant ($P<0.01$). As more striking evidence, the addition of KU55933 significantly attenuated the increased number of GFP-positive cells caused by rVpr (Figure 6c, right panel) ($P<0.01$). Data indicate that ATM is a critical molecule for the Vpr-induced enhancement of HR.

Discussion

Vpr induces DSBs and enhances HR

In this study, we showed that Vpr activates the ATM-dependent signal pathway involving Chk2 phosphorylation with focus formation of Rad51, BRCA1 and γ-H2AX. We previously reported that Vpr increases the rate of gene amplification (Shimura *et al*., 1999a), and a subsequent analysis by fluorescence *in situ* hybridization of amplified DNA suggested that a bridge-breakage fusion cycle, possibly triggered by DSBs (Ishizaka *et al*., 1995), was a relevant mode of Vpr-induced gene amplification. Data shown in the present study well supports our expectation that Vpr enhances gene amplification by causing DSBs (Shimura *et al*., 1999a).

We observed that the frequency of HR increased in response to Vpr. We examined the rate of HR by two systems measuring extrachromosomal recombination (Slebos and Taylor, 2001) and intrachromosomal recombination (Pierce *et al*., 1999). Both systems detect cells that are positive for GFP generated by gene conversion. Although it has been claimed that these two modes of HR do not always equally detect cellular recombinogenic conditions, our present data revealed that both systems detected the effects of Vpr on HR. It is interesting to note that the intrachromosomal recombination system used in the current study detects HR at

the specific site in the genome, where DSB is induced by expressing I-*Sce*I, a rare-cutting enzyme (Anglana and Bacchetti, 1999). We used two cell lines, both of which contained reporter constructs that were competent for a short tract gene conversion (Pierce *et al.*, 1999; Supplementary information 1), and we reproducibly detected enhancement of HR after treatment with Vpr. Data suggest that Vpr has an indirect effect on HR, indicating that DBSs at one locus contribute to trans-activation of HR at a different site.

In response to Vpr-induced DSBs, BRCA1 and RPA accumulated as foci (Figure 2b), and the association of Rad51 and p53 in the chromatin fraction was eliminated (Figure 3a and b). It has been reported that p53 associates with several proteins including BLM, BRCA1, BRCA2, Rad52 and RPA (Yamaguchi-Iwai

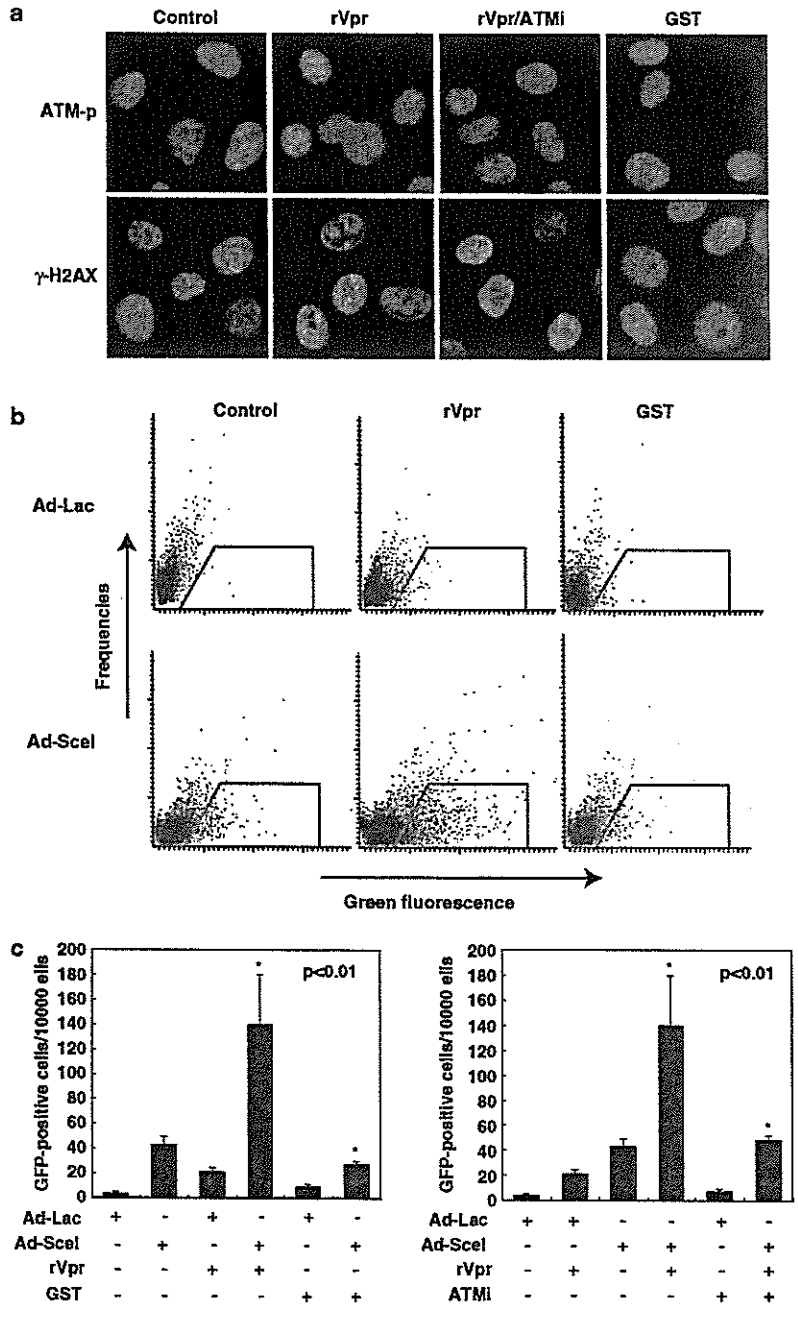

et al., 1998; Marmorstein *et al.*, 1998; Zhang *et al.*, 1998; Linke *et al.*, 2003; Sengupta *et al.*, 2003) and inhibits the Rad51-dependent HR (Cromie *et al.*, 2001; Linke *et al.*, 2003). When DSBs were induced, the association of p53 and Rad51 was prevented by an unknown mechanism. As the reduction of Rad51 and p53 interaction was also observed after irradiation (Figure 3c), it is likely that the Vpr-activated DNA-damage signaling overlaps with the cellular signals evoked by irradiation.

Biological relevance of Vpr-induced DSBs and HR for HIV-1 infection

Vpr expression enhances the rate of HR, but several reports suggest that NHEJ rather than HR contributes to viral infection (Daniel *et al.*, 1999; Li *et al.*, 2001; Jeanson *et al.*, 2002; Lau *et al.*, 2005). Additionally, Rad52, a cellular component of HR, was shown to work as a suppressive factor for HIV-1 transduction (Lau *et al.*, 2004). Together with data that the deletion of genes involved in HR, such as XRCC2 or XRCC3, did not alter the rate of viral integration (Chan *et al.*, 2004), it seems that upregulation of HR by Vpr does not by itself contribute to viral transduction.

In contrast, chemical compounds that generate DSBs increase the rate of integration of viral DNA into the host genome (Groschel and Bushman, 2005). This phenomenon has been explained by delayed progression at the G2/M phase due to DSBs. Additionally, caffeine and caffeine-related methylxanthines are known to impair HIV-1 infection (Nunnari *et al.*, 2005), and an ATM inhibitor, KU55933, is known to decrease the integration of viral DNA into host genome (Lau *et al.*, 2005). These observations suggest that a DSB-induced cellular signal, not HR, is important for viral integration, and that Vpr-induced DSB contributes to efficient viral integration in an ATM-dependent manner. An important issue to clarify is how cellular signals activated by ATM contribute to increased viral integration.

Possible mechanism of Vpr-induced DSBs and cell cycle abnormality

The mechanism of Vpr-induced DSBs is presently obscure. In the previous work, we showed that DSBs are induced by incubating isolated nuclei with purified recombinant Vpr protein (Tachiwana *et al.*, 2006). A purified Vpr possessed DNA binding activity, but it did not show any nuclease activity or activity of nicking DNAs. Additionally, Vpr is present in the chromatin fraction (Ishizaka, unpublished results, Lai *et al.*, 2005), implying the possibility that Vpr induces DSBs by modifying a chromatin structure to allow nucleases easy access. Another possibility is that Vpr associates with uncharacterized nuclease and recruits its activity to the vicinity of chromosomes. Studies are ongoing to identify cellular factor(s) that facilitate recruitment of Vpr to chromatin and induction of DSBs.

It is commonly accepted that Vpr-induced cell cycle abnormality is observed at the G2/M phase but not at the G1/S phase (Mahalingam *et al.*, 1998). Actually, we observed cellular accumulation at the G2/M phase in MIT-23 cells when Vpr expression was initiated (Shimura *et al.*, 1999b). Our present observation on the activation of ATM-dependent signal pathway by Vpr envisages that Vpr-induced cell cycle abnormality depends on ATM activation. A recent study, however, has shown that the ATR–Chk1 pathway, but not ATM–Chk2, is necessary for Vpr-induced G2 arrest (Roshal *et al.*, 2003; Zimmerman *et al.*, 2004). One possible explanation is that DSB-induced G2 arrest, for example, by X-ray irradiation largely depends on ATR-dependent signaling (Brown and Baltimore, 2003). The molecular linkage between ATM activation by Vpr and Vpr-induced cell cycle abnormality, however, needs to be carefully investigated.

Impact of Vpr-induced DSBs on the mechanism of tumor development in HIV-1-positive patients

We showed that DSBs and an increased rate of HR were induced when rVpr was added to the culture medium exogenously (Figure 6). Recently, we also found that Vpr is present in serum of HIV-1-positive patients (Levy *et al.*, 1994) at the concentration of about 0.7 nM (Hoshino *et al.*, submitted). In the current study, we used 3.7 nM of rVpr to obtain the definite activity inducing DSBs, but it would be possible that the high concentration of Vpr is present in the foci of HIV-1 infection, suggesting that DSBs can be generated in the cells within HIV-1-positive patients. The finding that Vpr is present in serum impacts the understanding of the mechanism of tumor development in HIV-1 positive patients. As reported by Biggar *et al.*, the relative risk of

Figure 6 Increased rate of intrachromosomal HR after treatment with rVpr. (**a**) Focus formation of γ-H2AX in cells treated with or without rVpr. HT1080 cells were incubated for 48 h in the presence of 3.7 nM of rVpr (see Materials and methods section), and subjected to immunohistochemical analysis by antibodies against ATM-p and γ-H2AX. Effects of KU55933 on rVpr-induced focus formation of these molecules are shown. As controls, the effects of the same concentration of GST, as an irrelevant bacteria-derived recombinant protein, are depicted (right panel). Their signals are shown as red spots in the nucleus (blue). (**b**) Effects of rVpr on HR. HT/DR–GFP cells (clone-1) were infected with Adβgal or Ad–SceI–NG with or without the addition of 3.7 nM of rVpr (middle panel). As a control, the same amount of GST was added to the culture (right panel). A region where no GFP-positive cells were present in control sample was first determined (upper left panel). Then numbers of cells in the gated areas were counted in the specimens after viral infection with or without treatment of recombinant proteins. (**c**) Vpr-induced increase of HR depends on ATM. Data obtained in Figure 6b were summarized (left panel). The addition of rVpr reproducibly enhanced the number of GFP-positive cells ($P<0.01$). Effects of ATM inhibitor (ATMi) were analysed by the same procedures shown in Figure 6b (right panel). KU55933 (ATMi) was added at a concentration of 1 mM at the same time that rVpr was added. As a control, the corresponding amount of dimethylsulfoxide (final concentration: 0.1% volume), which was used as a solvent for the compound, was included. ATMi significantly inhibited the rate of HR ($P<0.01$).

malignancy in AIDS patients was estimated to be 60- to1000-fold higher than healthy controls (Mayer *et al.*, 1995; Biggar *et al.*, 1996; Straus, 2001). Although it has been thought that an impaired cellular immunity under AIDS conditions permits the development of tumorigenesis (Knowles, 2003), recent observations indicate that non-AIDS-defining malignancies, tumors found in HIV-1-positive patients who have no deteriorated cellular immunity, are frequently observed in HIV-1-positive patients (Herida *et al.*, 2003; Burgi *et al.*, 2005; Lim and Levine, 2005). As antiretroviral therapy can effectively protect patients from severe infectious diseases (Chadburn and Cesarman, 1997; Elenitoba-Johnson and Jaffe, 1997), development of malignant tumors will be a critical prognostic factor of HIV-1 positive patients in the future. More precise study is required to clarify the molecular linkage of Vpr and malignant transformation.

Materials and methods

Cell culture and establishment of HT/DR-GFP

HT1080, a human fibrosarcoma cell line (JCRB9113; the Healthy Science Research Resources Bank), and its sublines were maintained at 37°C and 5% CO_2 in Dulbecco's modified Eagles medium (D-MEM) that was supplemented with 10% fetal bovine serum (FBS). The MIT-23 cell line was derived from HT1080 cells, in which Vpr expression is controlled by a tetracycline promoter, as described by Shimura *et al.* (1999b). For Vpr induction, 3 μg/ml DOX (Sigma, St Louis, MO, USA) was used. To obtain HT/DR-GFP, HT1080 cells were transfected with an inactive GFP expression cassette plasmid (pDR-GFP) and selected by puromycin (1 μg/ml), and clonal cell lines were established.

HIV infection

We used pseudotyped viruses that were defective for an envelope protein with *vpr* (R^+) or without *vpr* (R^-). HIV vectors were produced by transient transfection of 293T cells (Tokunaga *et al.*, 2001; Shimura *et al.*, 2005). The pNL-Luc-E^-R^+ or pNL-Luc-E^-R^- plasmid was co-transfected with pHIT/G using the transfection reagent Fugene-6 (Roche, Tokyo, Japan). Virus supernatants were collected at 48 h post-transfection. The harvested supernatants were centrifuged at 120 *g* for 5 min and stored at −80°C. Viral titers were measured by p24 ELISA (ZeptoMetrix). The virus was diluted in D-MEM supplemented with 10% FBS and used to infect HT1080 cells at a multiplicity of infection (MOI) of 0.8, which yielded about 80% of cells that were positive for luciferase expression (data not shown).

Protein analyses

The cells were washed with phosphate-buffered saline (PBS) and resuspended in radio-immunoprecipitation assay buffer composed of 50 mM Tris-HCl, 1% NP-40, 0.25%. sodium deoxycholate, 150 mM NaCl, 1 mM EGTA, 1 mM phenylmethysulfonyl fluoride, 1 μg/ml protease inhibitor mix, 1 mM Na_2VO_3 and 1 mM NaF. The cell suspension was sonicated. To fractionate chromatin fractions, cells were suspended in Buffer N (15 mM Tris-HCl (pH 7.5), 60 mM KCl, 15 mM NaCl, 5 mM $MgCl_2$, 1 mM $CaCl_2$, 1 mM DTT, 2 mM Na_2VO_3, 250 mM sucrose, protease inhibitors) with 0.6% NP-40. Cells were incubated on ice for 5 min followed by centrifugation (2000 *g*) to separate cytoplasmic proteins from nuclei. Isolated nuclei were then washed twice with Buffer N followed by resuspension in Lysis buffer (10 mM PIPES (pH 6.5), 10 mM EDTA, protease inhibitors) and centrifugation (6000 *g*) to extract soluble nuclear proteins. Finally, chromatin was resuspended in Lysis buffer and shared by sonication on ice to extract chromatin-bound proteins. The protein concentration was determined using the BCA protein assay reagent kit (Pierce). A 100-μg aliquot of protein from each cell extract was separated on 10% SDS–PAGE. Specific primary antibodies of p53 (Calbiochem), Chk2, ATM-S1981 (ATM-p), H2AX-S139 (γ-H2AX) and histone H3 (Upstate), Chk2-T68 (Chk2-p) and p53-S15 (p53-p) (Cell Signaling) were used for analysis. A monoclonal antibody to Vpr, 8D1 (IgG2a) was raised by immunization of a full-length Vpr peptide (Peptide Institute).

Immunoprecipitation was performed using 500 μg of protein mixed with 2 μg of anti-p53 protein-specific IgG-beads. Ternary complexes of protein A–antibody–antigen were collected by centrifugation and washed three times. The immunoprecipitates were subjected to SDS–PAGE followed by Western blot analysis. To obtain a rabbit antibody to RAD51, the human Rad51 protein was expressed as a recombinant protein in the *Escherichia coli* strain JM109 (DE3) (Kagawa *et al.*, 2001), and was purified as described previously (Kurumizaka *et al.*, 1999). Detection of target proteins was with an enhanced chemiluminescence detection system (Amersham Biosciences).

Immunostaining

The cells were washed with PBS and fixed with 2% paraformaldehyde in PBS and ice-cold methanol. The fixed cells were permeabilized with 0.2% Triton X-100 in PBS for 5 min. After treatment with PBS containing 10% goat serum for 30 min, the cells were incubated with primary antibodies that included rabbit polyclonal antibodies against Rad51 (1:400), mouse monoclonal antibodies against ATM-p (1:100) and γ-H2AX (1:100) (Upstate) and mouse monoclonal antibodies against BRCA1 (1:300) and RPA (1:1000) (Lab Vision). After 1 h of incubation at 37°C, secondary antibodies conjugated with Alexa 546 (1:1000; Molecular Probes, Eugene, OR, USA) were added for 1 h at 37°C. The slides were mounted in an anti-fade solution (KPL) and analysed by fluorescence microscopy.

Homologous recombination assay

The rate of extrachromosomal HR was assessed as previously described (Slebos and Taylor, 2001). HT1080 cells were co-transfected with pBHRF and pcDNA3.1/Vpr or pcDNA3.1 (Invitrogen). pBHRF encodes both a truncated GFP and full-length BFP. In the absence of HR, only BFP is expressed. However, HR between the BFP and truncated GFP results in the creation of a functional GFP. The green and blue fluorescence levels were examined simultaneously using a Vantage flow cytometer (Becton-Dickinson) equipped with a 488-argon laser (GFP) and a UV (350–360 nm) laser (BFP). *vpr* was derived from a NL4-3 clone (Adachi *et al.*, 1986). Each experiment was performed at least three times, and statistical analysis was carried out by Student's *t*-test.

The rate of intrachromosomal HR was assessed as reported in human glioma cells (Pierce *et al.*, 1999). Upon infection with Ad-I-Sce-I, a kind gift from Dr F Graham (McMaster University, Canada) or Ad-Lac8 (a gift from Dr I Saito, Tokyo University) as a control, GFP-positive cells as a result of HR were analysed. KU55933, a gift from Dr M O'Connor (KuDOS Pharmaceuticals, England), was dissolved in dimethylsulfoxide (DMSO). GFP was analysed with laser scanning cytometer

(LSC; Olympus, Tokyo, Japan) (Huang *et al*., 2006). Cells cultured in cover slide were immersed in 0.2% Triton X-100 in PBS for 10 min. The slides were then incubated with anti-GFP antibody (1:100; Molecular Probes) before adding Alexa Fuor 488 conjugated secondary antibody (1:400; Molecular Probes). Green fluorescence emission was measured with LSC. The integrated fluorescence was measured in 10000 cells for each sample. Each experiment was repeated three times, and statistical significance was examined.

Expression and purification of rVpr

rVpr was expressed in BL-21 codon plus (Stratagene) as a GST fusion protein and purified using glutathione column chromatography, as described (Hoshino *et al*., submitted). Vpr eluted after precision treatment was applied to an affinity column coupled with a monoclonal antibody to Vpr, 8D1. After washing, Vpr was eluted with 100 mM Hepes buffer (pH 2.5), and immediately neutralized with 1 M Hepes buffer (pH 8.0). The concentration of rVpr was measured by an enzyme-linked immunosorbent assay version-1 by using two antibodies against Vpr, a monoclonal antibody (8D1), and a polyclonal antibody raised against a peptide of the carboxy-terminus of Vpr (IBL).

Acknowledgements

We are grateful to Dr T Takemori (National Institute of Infectious Diseases, Japan) to help for analysis by a Vantage flow cytometer. We also thank to Riken BRC for control adenovirus, AxCALac8, and HT1080 cells. Drs Slebos (National Institute of Environmental Health Science, USA), Jasin M (Memorial Sloan-Kettering Cancer Center, USA), Graham F (McMaster University, Canada), and Saito I (Institute of Medical Sciences, of Tokyo University, Japan) kindly provided us with pBHRF, pDR-GFP, adenovirus of I-*Sce*I, and AxCALac8, respectively. We also thank to O'Connor M (KuDOS pharmaceuticals, England) for KU55933. This work was supported by a Grant-in-Aid for Scientific Research from the Ministry of Health, Labor and a Grant for research on Health Sciences focusing on Drug Innovation. Dr Nakai-Murakami is a research resident supported by the Japan Health Sciences Foundation.

References

Abraham RT. (2001). *Genes Dev* **15**: 2177–2196.
Anglana M, Bacchetti S. (1999). *Nucleic Acids Res* **27**: 4276–4281.
Bartz SR, Rogel ME, Emerman M. (1996). *J Virol* **70**: 2324–2331.
Bertrand P, Saintigny Y, Lopez BS. (2004). *Trends Genet* **20**: 235–243.
Biggar RJ, Rosenberg PS, Coté T, Multistate AIDS/Cancer Match Study Group. (1996). *Int J Cancer* **68**: 754–758.
Brown EJ, Baltimore D. (2003). *Genes Dev* **17**: 615–628.
Bukrinsky M, Adzhubei A. (1999). *Rev Med Virol* **9**: 39–49.
Burgi A, Brodine S, Wegner S, Milazzo M, Wallace MR, Spooner K *et al*. (2005). *Cancer* **104**: 1505–1511.
Chadburn A, Cesarman E, Knowles DH. (1997). *Semin Diagn Pathol* **14**: 15–26.
Cromie GA, Connelly JC, Leach DRF. (2001). *Mol Cell* **8**: 1163–1174.
Daniel R, Greger JG, Katz RA, Taganov KD, Wu X, Kappes JC *et al*. (2004). *J Virol* **78**: 8573–8581.
Daniel R, Kao G, Tagarov K, Greger JG, Favorova O, Merkel G *et al*. (2003). *Proc Natl Acad Sci USA* **100**: 4778–4783.
Daniel R, Katz RA, Skalka AM. (1999). *Science* **284**: 644–647.
Daniel R, Marusich E, Argyris E, Zhao RY, Skalka AM, Pomerantz RJ. (2005). *J Virol* **79**: 2058–2065.
Dong Y, Hakimi MA, Chen X, Kumaraswamy E, Cooch NS, Godwin AK *et al*. (2003). *Mol Cell* **12**: 1087–1099.
Elder RT, Benko Z, Zhao Y. (2002). *Front Biosci* **7**: d349–d357.
Elenitoba-Johnson KS, Jaffe ES. (1997). *Semin Diagn Pathol* **14**: 35–47.
Goh WC, Rogel ME, Kinsey CM, Michael SF, Fultz PN, Nowak MA *et al*. (1998). *Nat Med* **4**: 65–71.
Groschel B, Bushman F. (2005). *J Virol* **79**: 5695–5704.
He J, Choe S, Walker R, Di Marzio PD, Morgan DO, Landau NR. (1995). *J Virol* **69**: 6705–6711.
Henklein P, Bruns K, Sherman MP, Tessmer U, Licha K, Kopp J *et al*. (2000). *J Biol Chem* **275**: 32016–32026.
Herida M, Mary-Krause M, Kaphan R, Cadranel J, Poizot-Martin IP, Rabaud C *et al*. (2003). *J Clin Oncol* **21**: 3447–3453.
Hoshino S, Sun B, Shimura M, Konishi M, Taguchi T, Segawa T *et al*. (2006). *submitted*.
Huang M-B, Weeks O, Zhao L-J, Saltarelli M, Bond VC. (2000). *J Neuro Viol* **6**: 202–220.
Huang X, Kurose A, Tanaka T, Traganos F, Dai W, Darzynkiewicz Z. (2006). *Cytometer A* **69A**: 222–229.
Ishizaka Y, Chernov MV, Burns CM, Stark GR. (1995). *Proc Natl Acad Sci USA* **92**: 3224–3228.
Yamaguchi-Iwai Y, Sonoda E, Buerstedde J-M, Bezzubova O, Morrison C, Takata M *et al*. (1998). *Mol Cell Biol* **18**: 6430–6435.
Jeanson L, Subra F, Vaganay S, Hervy M, Marangoni E, Bourhis J *et al*. (2002). *Virology* **300**: 100–108.
Jenkins Y, McEntee M, Weis K, Greene WC. (1998). *J Cell Biol* **143**: 875–885.
Kagawa W, Kurumizaka H, Ikawa S, Yokoyama S, Shibata T. (2001). *J Biol Chem* **276**: 35201–35208.
Khanna KK, Jackson SP. (2001). *Nat Genet* **27**: 247–254.
Khanna KK, Lavin MF, Jackson SP, Mulhern TD. (2001). *Cell Death Differ* **8**: 1052–1065.
Knowles DM. (2003). *Hematol Oncol Clin N Am* **17**: 785–820.
Kurumizaka H, Aihara H, Kagawa W, Shibata T, Yokoyama S. (1999). *J Mol Biol* **291**: 537–548.
Lai M, Zimmerman ES, Planelles V, Chen J. (2005). *J Virol* **79**: 15443–15451.
Lau A, Kanaar R, Jackson SP, O'Connor MJ. (2004). *EMBO J* **23**: 3421–3429.
Lau A, Swinbank KM, Ahmed PS, Taylor DL, Jackson SP, Smith GCM *et al*. (2005). *Nat Cell Biol* **7**: 493–500.
Laurence J, Astrin SM. (1991). *Proc Natl Acad Sci USA* **88**: 7635–7639.
Levy DN, Refaeli Y, MacGregor RR, Weiner DB. (1994). *Proc Natl Acad Sci USA* **91**: 10873–10877.
Li L, Olvera JM, Yoder KE, Mitchell RS, Butler SL, Lieber M *et al*. (2001). *EMBO J* **20**: 3272–3281.
Lim ST, Levine AM. (2005). *Curr HIV/AIDS Rep* **2**: 146–153.
Linke SP, Sengupta S, Khabie N, Jeffries BA, Buchhop S, Miska S *et al*. (2003). *Cancer Res* **63**: 2596–2605.
Mahalingam S, Ayyavoo V, Patel M, Kieber-Emmons T, Kao GD, Muschel RJ *et al*. (1998). *Proc Natl Acad Sci USA* **95**: 3419–3424.
Marmorstein LY, Ouchi T, Aaronson SA. (1998). *Proc Natl Acad Sci USA* **95**: 13869–13874.

Mayer V, Ebbesen P, Zachar V. (1995). *Eur J Cancer Prev* **4**: 211–212.
Nunnari G, Argyris E, Fang J, Mehlman KE, Pomerantz RJ, Daniel R. (2005). *Virology* **335**: 177–184.
O'Connell MJ, Walworth NC, Carr AM. (2000). *Trends Cell Biol* **10**: 296–303.
Pierce AJ, Johnson RD, Thompson LH, Jasin M. (1999). *Gene Dev* **13**: 2633–2638.
Roshal M, Kim B, Zhu Y, Nghiem P, Planelles V. (2003). *J Biol Chem* **278**: 25879–25886.
Sawaya BE, Khalili K, Mercer WE, Denisova L, Amini S. (1998). *J Biol Chem* **273**: 20052–20057.
Sengupta S, Linke SP, Pedeux R, Yang Q, Farnsworth J, Garfield SH *et al.* (2003). *EMBO J* **22**: 1210–1222.
Shiloh Y. (2001). *Curr Opin Genet Dev* **11**: 71–77.
Shimura M, Onozuka Y, Yamaguchi T, Hatake K, Takaku F, Ishizaka Y. (1999a). *Cancer Res* **59**: 2259–2264.
Shimura M, Tanaka Y, Nakamura S, Minemoto Y, Yamashita K, Hatake K *et al.* (1999b). *FASEB J* **13**: 621–637.
Shimura M, Tokunaga K, Konishi M, Sato Y, Kobayashi C, Sata T *et al.* (2005). *AIDS* **19**: 1434–1438.
Slebos RC, Taylor JA. (2001). *Biochem Biohpys Res Commun* **281**: 212–219.
Straus DJ. (2001). *Curr Oncol Rep* **3**: 260–265.
Tachiwana H, Shimura M, Nakai-Murakami C, Tokunaga K, Takizawa Y, Sata T *et al.* (2006). *Cancer Res* **66**: 627–631.
Taguchi T, Shimura M, Osawa Y, Suzuki Y, Mizoguchi I, Niino K *et al.* (2004). *Biochem Biophys Res Commun* **320**: 18–26.
Tokunaga K, Greenberg ML, Morse MA, Cumming RI, Lyerly HK, Cullen BR. (2001). *J Virol* **75**: 6776–6785.
van Gent DC, Hoeijmakers JHJ, Kanaar R. (2001). *Nat Rev Genet* **2**: 196–206.
Waldman AS, Liskay RM. (1987). *Proc Natl Acad Sci USA* **84**: 5340–5344.
West SC. (2003). *Nat Rev Mol Cell Biol* **4**: 1–11.
Yoon D, Wang Y, Stapleford K, Wiesmüller L, Chen J. (2004). *J Mol Biol* **336**: 639–654.
Yuan H, Kamata M, Xie Y-M, Chen ISY. (2004). *J Virol* **78**: 8183–8190.
Zhang H, Somasundaram K, Peng Y, Tian H, Zhang H, Bi D, Weber BL *et al.* (1998). *Oncogene* **16**: 1713–1721.
Zimmerman ES, Chen J, Andersen JL, Ardon O, DeHart JL, Blackett J *et al.* (2004). *Mol Cell Biol* **24**: 9286–9294.

Supplementary Information accompanies the paper on the Oncogene website (http://www.nature.com/onc).

Published online 31 August 2006

Nucleic Acids Research, 2006, Vol. 34, No. 16 4429–4437
doi:10.1093/nar/gkl562

Stimulation of Dmc1-mediated DNA strand exchange by the human Rad54B protein

Naoyuki Sarai[1,2], Wataru Kagawa[1], Takashi Kinebuchi[1], Ako Kagawa[1], Kozo Tanaka[3], Kiyoshi Miyagawa[4], Shukuko Ikawa[5], Takehiko Shibata[5], Hitoshi Kurumizaka[1,6,*] and Shigeyuki Yokoyama[1,2,7,*]

[1]RIKEN Genomic Sciences Center, 1-7-22 Suehiro-cho, Tsurumi, Yokohama 230-0045, Japan, [2]Department of Biophysics and Biochemistry, Graduate School of Science, University of Tokyo, 7-3-1 Hongo, Bunkyo-ku, Tokyo 113-0033, Japan, [3]School of Life Sciences, University of Dundee, Wellcome Trust Biocentre, Dundee DD1 5EH, UK, [4]Center for Disease Biology and Integrative Medicine, Faculty of Medicine, University of Tokyo, 7-3-1 Hongo, Bunkyo-ku, Tokyo 113-0033, Japan, [5]RIKEN Discovery Research Institute, Wako-shi, Saitama 351-0198, Japan, [6]Graduate School of Science and Engineering, Waseda University, 3-4-1 Okubo, Shinjuku-ku, Tokyo 169-8555, Japan and [7]RIKEN Harima Institute at SPring-8, 1-1-1 Kohto, Mikazuki-cho, Sayo, Hyogo 679-5148, Japan

Received May 2, 2006; Revised July 18, 2006; Accepted July 19, 2006

ABSTRACT

The process of homologous recombination is indispensable for both meiotic and mitotic cell division, and is one of the major pathways for double-strand break (DSB) repair. The human Rad54B protein, which belongs to the SWI2/SNF2 protein family, plays a role in homologous recombination, and may function with the Dmc1 recombinase, a meiosis-specific Rad51 homolog. In the present study, we found that Rad54B enhanced the DNA strand-exchange activity of Dmc1 by stabilizing the Dmc1–single-stranded DNA (ssDNA) complex. Therefore, Rad54B may stimulate the Dmc1-mediated DNA strand exchange by stabilizing the nucleoprotein filament, which is formed on the ssDNA tails produced at DSB sites during homologous recombination.

INTRODUCTION

Chromosomal DNA is exposed to various DNA-damaging agents and sustains damage that induces genomic instability. A double-strand break (DSB) is caused by ionizing radiation, cross-linking reagents, oxidative stress and DNA replication failure. If the DSB is left unrepaired, then cell death occurs (1–4). Homologous recombination is one of the major DSB repair pathways. This repair pathway is essentially error-free, since a homologous region of the undamaged sister chromatid is used as the template for repair. In contrast to the mitotic DSB repair pathway, meiotic cell division involves homologous recombination between homologous chromosomes, but not between sister chromatids. This preferential recombination between homologous chromosomes is initiated by the formation of a programmed DSB and ensures correct chromosomal segregation at meiosis I through the formation of chiasmata, which physically connect homologous chromosomes (5,6). Thus, homologous recombination is important to maintain the integrity of the chromosome in both mitotic and meiotic cells.

In homologous recombination, a single-stranded DNA (ssDNA) tail, produced at the DSB site, is incorporated into a nucleoprotein complex called the presynaptic filament. This presynaptic filament catalyzes homologous pairing and strand exchange with an intact homologous region of the double-stranded DNA (dsDNA) molecule. The bacterial RecA protein is known to form helical presynaptic filaments and to play central roles in homologous recombination (7–12). In eukaryotes, two homologs of RecA, the Rad51 and Dmc1 proteins, which are conserved from yeast to human, are assumed to fulfill this role. Rad51 is expressed in both meiotic and mitotic cells, whereas the expression of Dmc1 is restricted to meiotic cells (13–16). Although previous biochemical studies demonstrated that Rad51 and Dmc1 have recombinational activities similar to those of RecA (17–22), other studies have also revealed that many ancillary factors, such as replication protein A (RPA), Rad52 and Rad54, significantly affect the activities of Rad51 and Dmc1 (23,24).

Rad54 is a member of the SWI2/SNF2 family of proteins, which have DNA-dependent ATPase activities and are involved in chromatin remodeling (25–31). Genetic studies revealed that Rad54-deficient cells are sensitive to DNA-damaging agents, such as ionizing radiation, methyl methanesulfonate (MMS) and mitomycin C (32). Rad54 utilizes the free energy from ATP hydrolysis to generate superhelical

*To whom correspondence should be addressed. Tel: +81 3 5286 8189; Fax: +81 3 5292 9211; Email: kurumizaka@waseda.jp
*Correspondence may also be addressed to Shigeyuki Yokoyama. Tel: +81 3 5841 4413; Fax: +81 3 5841 8057; Email: yokoyama@biochem.s.u-tokyo.ac.jp

torsion into dsDNA by translocating on the DNA (33,34). Furthermore, yeast Rad54 promotes the assembly and disassembly of the Rad51 nucleoprotein filament, and both yeast and human Rad54 stimulate the Rad51-mediated homologous pairing activity by directly binding to Rad51 (35–37).

Recent studies showed that the human Rad54B protein, a homolog of Rad54, interacts with the human Rad51and Dmc1 proteins, and stimulates the homologous pairing activity mediated by these proteins (22,38). Similar to Rad54, human Rad54B is a DNA-dependent ATPase (39) and is expressed in both mitotic and meiotic cells (40). However, genetic studies revealed that human Rad54B-deficient cells are not overly sensitive to ionizing radiation, MMS and cisplatin (41). Furthermore, the human Rad54B-deficient cells are also proficient in mitotic sister chromatid exchange (41). On the other hand, a severe reduction in targeted integration frequency was detected in the Rad54B-deficient cells (41). These characteristics are different from those of Rad54, indicating that Rad54B may have a unique role in homologous recombination.

To understand the function of Rad54B in homologous recombination, in the present study, we purified the human Rad54B protein, which was overexpressed in insect cells and biochemically characterized it. The purified Rad54B protein bound to the ATPase domain of Dmc1. Furthermore, Rad54B stimulated the DNA strand exchange mediated by Dmc1 and stabilized the Dmc1–ssDNA complex. Therefore, Rad54B may stimulate the Dmc1-mediated strand exchange by stabilizing the Dmc1–ssDNA nucleoprotein filament during homologous recombination.

MATERIALS AND METHODS

Protein purification

The human Rad54B cDNA was subcloned from pFastBac HTC (Invitrogen) into pFastBac 1 (Invitrogen), and a recombinant human Rad54B baculovirus was generated as described previously (39). High Five insect cells were infected with human Rad54B at a multiplicity of infection of 1, and were harvested after 72 h. The cells were resuspended in buffer A (pH 7.5), containing 50 mM Tris–HCl, 0.6 M KCl, 2 mM 2-mercaptoethanol (2ME), 10% sucrose and 10 mM EDTA, and were disrupted by sonication. The cell debris was removed by centrifugation for 40 min at 100 000 *g*, and the lysate was treated with ammonium sulfate (0.21 g/ml). The protein precipitate was redissolved in 50 ml of buffer B (pH 7.5), containing 20 mM HEPES–KOH, 0.2 M KCl, 0.5 mM EDTA, 2 mM 2ME, 10% glycerol and 0.01% NP-40. The protein solution was mixed with 8 ml of phosphocellulose column matrix at 4°C for 1 h, and then the mixture was packed into an Econo-column (Bio-Rad). After washing with 20 CV of buffer B, the Rad54B protein was eluted by a 20 CV linear gradient from 0.2 to 1.0 M KCl. The Rad54B protein was dialyzed against buffer C (pH 7.4), containing 20 mM potassium phosphate, 0.15 M KCl, 2 mM 2ME, 10% glycerol and 0.01% NP-40, and then was mixed with 6 ml of Q-Sepharose (GE Healthcare) column matrix at 4°C for 1 h. The proteins in the Q-Sepharose flow-through fraction were mixed with 6 ml of SP–Sepharose (GE Healthcare) column matrix at 4°C for 1 h, and then the mixture was packed into an Econo-column. The column was washed with 20 CV of buffer C and was eluted with a 20 CV linear gradient from 0.15 to 1.0 M KCl. The peak fractions were dialyzed against buffer D (pH 7.4), containing 20 mM potassium phosphate, 0.2 M KCl, 2 mM 2ME, 10% glycerol and 0.01% NP-40, and were loaded on to a 1 ml hydroxyapatite column. The column was washed with 20 CV of buffer D and was eluted with a 20 CV linear gradient from 20 to 300 mM potassium phosphate. The peak fractions of the Rad54B proteins were collected, dialyzed against buffer B and stored at −80°C.

The human Rad51 protein was purified as described previously (42), with the inclusion of a spermidine precipitation purification step. Briefly, after the removal of the His_6-tag, the Rad51 protein was dialyzed at 4°C against buffer E (pH 7.5), containing 100 mM Tris–acetate, 7 mM spermidine HCl and 5% glycerol. The Rad51 precipitate was collected by centrifugation and resuspended in buffer F (pH 7.0), which contained 100 mM potassium phosphate, 0.15 M NaCl, 1 mM EDTA, 2 mM 2ME and 10% glycerol, and was purified on a 1 ml Mono Q column (GE Healthcare) as described previously.

The human Dmc1, Dmc182–340 and RPA proteins were purified as described previously (43–45). The concentrations of the purified proteins were determined with a Bio-Rad protein assay kit, using BSA as the standard.

DNA substrates

The φX174 circular ssDNA (5386 bases) and replicative form I DNA were purchased from New England Biolabs and Life Technologies. For the assays of strand exchange and protein transfer between DNA molecules, the replicative form I DNA was linearized with ApaL I. To perform the gel mobility shift assay for the protein transfer between ssDNA molecules, the φX174 circular ssDNA was cut to ~500 base fragments by an incubation at 98°C. The 120mer oligonucleotide, called SAT-120 (5′-ATTTC TTCAT TTCAT GCTAG ACAGA AGAAT TCTCA GTAAC TTCTT TGTGC TGTGT GTATT CAACT CACAG AGTGG AACGT CCCTT TGCAC AGAGC AGATT TGAAA CACTC TTTTT GTAGT-3′), was used in the pull down assay for the protein transfer between ssDNA molecules. All DNA concentrations are expressed as molar nucleotide concentrations.

Protein–protein binding assay

Rad51, Dmc1, Dmc182–340 and BSA were covalently conjugated to Affi-Gel 15 beads (100 µl; Bio-Rad), according to the manufacturer's instructions. The unbound proteins were removed by washing the beads for five times with binding buffer G (pH 7.5), which contained 20 mM HEPES–KOH, 0.15 M KCl, 0.5 mM EDTA, 2 mM 2ME, 10% glycerol and 0.05% Triton X-100. To block the residual active ester sites, ethanolamine (pH 8.0) was added to a final concentration of 100 mM, and the resin was incubated at 4°C for 1 h. After washing the resin three times with 500 µl of buffer G, the Affi-Gel 15-protein matrices were adjusted to 50% slurries with buffer G and were stored at 4°C.

For the binding assay, the Affi-Gel 15-protein slurry (20 µl) was mixed with 20 µg of Rad54B at room temperature for 2 h. The Affi-Gel 15-protein beads were then washed five

times with 500 µl of buffer G. SDS–PAGE sample buffer (2-fold) was mixed directly with the washed beads. After heating the mixture at 98°C for 5 min, the proteins were fractionated by 4–20% gradient SDS–PAGE. Bands were visualized by Coomassie brilliant blue staining.

Immunoprecipitation experiments

The human Dmc1 and Rad54B cDNA were subcloned into the same pFastBac Dual vector (Invitrogen), and a recombinant baculovirus containing both the Dmc1 and Rad54B genes was generated as described previously. Sf9 insect cells were infected with this baculovirus, and were harvested after 48 h. The cells were then resuspended in buffer G, and were disrupted by sonication. The resulting cell lysate was incubated with 10 µl of anti-Dmc1 or Rad54B antibody conjugated to rProtein A–Sepharose Fast Flow (GE Healthcare) at 4°C for 1 h. The beads were washed five times with 500 µl of phosphate-buffered saline containing 1% NP-40, and were eluted by the addition of SDS–PAGE sample buffer (2-fold). The eluted fractions were separated by 4–20% gradient SDS–PAGE, and were blotted on to a polyvinylidene fluoride membrane. The proteins transferred on the membrane were analyzed by immunoblotting. The rabbit anti-Dmc1 antibody was prepared in this study, and the preparation of the rabbit anti-Rad54B antibody was described previously (46).

DNA strand exchange assay

All of the experiments were performed in a final volume of 10 µl of buffer H, containing 35 mM Tris–HCl (pH 7.8), 1 mM DTT, 2 mM ATP, 2.5 mM $MgCl_2$, 20 mM creatine phosphate and 75 µg/ml creatine kinase. The reactions were started by incubating 7.5 µM Dmc1 with 30 µM φX174 circular ssDNA at 37°C for 5 min. Then, 2 µM RPA and 200 mM KCl were added, and after a 5 min incubation at 37°C, 22 µM φX174 linear dsDNA and 0.025–1.6 µM Rad54B were incorporated to initiate the reaction. After incubations at 37°C for the indicated times, the reactions were terminated by the addition of 0.5% SDS and 700 µg/ml proteinase K, followed by an incubation at 37°C for 20 min. After 10-fold loading dye was added, the products were resolved by 1% agarose gel electrophoresis in TAE buffer at 3.3 V/cm for 2.5 h, and were visualized by staining with ethidium bromide.

Protein transfer assay (1): using biotinylated-ssDNA molecules and streptavidin beads

Dmc1 (5 µM) was incubated for 5 min at 37°C with 20 µM SAT-120 (120mer) labeled with biotin at the 5′ end, in 80 µl of buffer I, containing 35 mM Tris–HCl (pH 7.8), 1 mM DTT, 2 mM ATP and 2.5 mM $MgCl_2$. The reaction mixture was then divided in two, and a 5 µl aliquot of Rad54B (200 nM) or buffer B was added. After an incubation at 37°C for 5 min, a 5 µl aliquot of φX174 circular ssDNA (2 mM) was added, and the reaction was incubated at 37°C for 2 h. The DNA–protein complexes were captured with 50 µl of ImmunoPure Immobilized Streptavidin Gel (PIERCE) equilibrated with buffer I with 0.1% Triton X-100. After an incubation at 4°C for 1 h, the reaction mixture was divided into the beads and the supernatant by centrifugation. After adding 2-fold SDS–PAGE sample buffer and heating the mixture at 98°C for 5 min, the supernatant was fractionated by 4–20% gradient SDS–PAGE. Bands were visualized by Coomassie brilliant blue staining.

Protein transfer assay (2): resolving protein–DNA complexes on agarose gels

For the assay, 10 µM Dmc1 was incubated with 20 µM φX174 circular ssDNA at 37°C for 5 min, in 80 µl of buffer H. The reaction mixture was then divided in two, and a 5 µl aliquot of Rad54B (200 nM) or buffer B was added. After an incubation at 37°C for 5 min, these mixtures were incubated with various concentrations of φX174 ssDNA fragments (0–200 µM) at 37°C for 2 h. After 10-fold loading dye was added, the products were resolved by 1% agarose gel electrophoresis in TAE buffer at 3.3 V/cm for 2.5 h and were visualized by staining with ethidium bromide.

Electron microscopic analysis

Dmc1 (10 µM) was incubated with 15 µM SAT-120 (120mer) at 37°C for 5 min, in 10 µl of buffer J, containing 25 mM Tris–HCl (pH 7.5), 1 mM DTT, 2 mM ATP and 5 mM $MgCl_2$. Then, 200 mM KCl was added, and after a 5 min incubation at 37°C, 0.4 µM Rad54B was incorporated. The protein–DNA complexes were fixed with 0.2% glutaraldehyde at 37°C for 10 min. After a 100-fold dilution with buffer J, the reaction mixture was negatively stained with 2% uranyl acetate. The complexes were observed with a JEOL JEM 2000FX electron microscope.

RESULTS

Purification of Rad54B and its interactions with Rad51 and Dmc1

First, we examined whether Rad54B physically interacts with Rad51 and Dmc1, because recent studies revealed that Rad54B interacts with these proteins (22,38), in contrast to our previous results (39). To do so, we newly subcloned Rad54B into pFastBac1, which lacks a His_6-tag site, and employed an improved Rad54B purification method. Rad54B was expressed in baculovirus-infected High Five insect cells. The cell lysate was treated with ammonium sulfate (Figure 1A, lane 2). The precipitate was redissolved and further purified by phosphocellulose column chromatography (Figure 1A, lane 3), Q-Sepharose column chromatography (Figure 1A, lane 4), SP–Sepharose column chromatography (Figure 1A, lane 5) and hydroxyapatite column chromatography (Figure 1A, lane 6). About 1 mg of purified Rad54B was obtained from 3 liters of High Five insect cell suspension culture.

To examine the interaction, Rad51 and Dmc1, separately conjugated on Affigel 15 beads (Rad51-beads and Dmc1-beads, respectively), were incubated with purified Rad54B, and the protein bound to either the Rad51 beads or the Dmc1 beads was detected by SDS–PAGE. As shown in Figure 1B, Rad54B interacted with both Dmc1 and Rad51 (lanes 3 and 4). These results are consistent with the previous data (22,38,46). Furthermore, Rad54B interacted with a Dmc1 mutant ($Dmc1_{82-340}$) lacking 81 amino acid residues

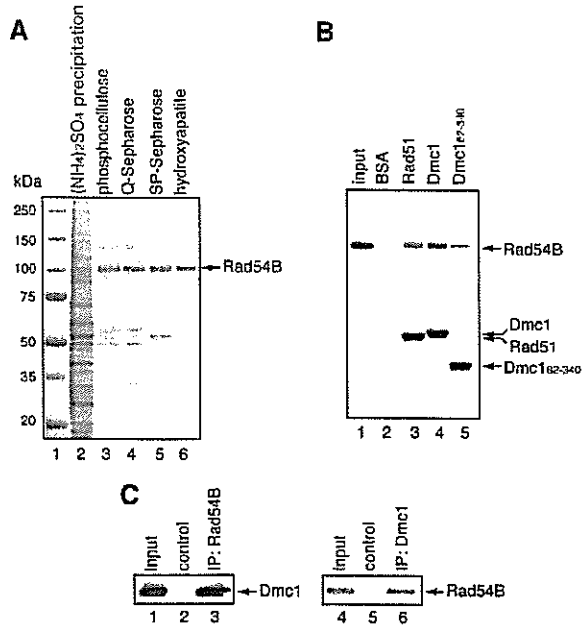

Figure 1. Rad54B purification and complex formation. (A) SDS–PAGE of the column fractions containing Rad54B. The proteins precipitated by ammonium sulfate (lane 2), the phosphocellulose peak fraction (lane 3), the Q-Sepharose flow-through (lane 4), the SP–Sepharose peak fraction (lane 5) and the hydroxyapatite peak fraction (lane 6) were fractionated on a 4–20% SDS–PAGE gel and stained with Coomassie brilliant blue. Lane 1 indicates the molecular mass markers. (B) Protein–protein interaction assay of Rad54B with Rad51, Dmc1 and $Dmc1_{82-340}$. Rad54B was mixed with either Rad51, Dmc1 or $Dmc1_{82-340}$ that was covalently conjugated to an Affi-Gel 15 matrix. After an incubation at room temperature, the Affi-Gel 15 matrices were washed with binding buffer, directly mixed with 2-fold SDS–PAGE sample buffer and fractionated on a 4–20% gradient SDS–PAGE gel. Lane 1 is one-tenth (2 μg) of the input proteins, lane 2 is the negative control using the Affi-Gel 15 matrix conjugated with BSA, lane 3 is the Affi-Gel 15 matrix conjugated with Rad51, lane 4 is the Affi-Gel 15 matrix conjugated with Dmc1 and lane 5 is the Affi-Gel 15 matrix conjugated with $Dmc1_{82-340}$. The bands were visualized by Coomassie brilliant blue staining. Notably, the Rad51, Dmc1 and $Dmc1_{82-340}$ proteins form multimers and thus, these proteins can indirectly associate with the Affi-Gel matrix via interactions with proteins crosslinked to the matrix. Rad51, Dmc1 and $Dmc1_{82-340}$ detected in lanes 3–5 represent fractions that were not covalently conjugated to the Affi-Gel beads. In contrast, BSA was not detected (lane 2), since BSA does not form multimers, and all proteins were covalently conjugated to the beads. (C) Immunoprecipitation (IP) experiments of Rad54B and Dmc1. Sf9 insect cells were infected with a baculovirus containing both the Dmc1 and Rad54B genes. The cells were lysed and subjected to immunoprecipitation with anti-Rad54B antibody (lane 3) or anti-Dmc1 antibody (lane 6). The precipitates were analyzed by immunoblotting. As negative control experiments, the cell lysate was incubated with normal IgG (lanes 2 and 5). Lanes 1 and 4 are one-tenth of the input cell lysate.

from the N-terminus (Figure 1B, lane 5). The region encompassing amino acids 82–340 of Dmc1 corresponds to the core ATPase domain (45), which is structurally conserved among the RecA-family proteins, such as eukaryotic Rad51 and Dmc1 (43,47,48), archaeal RadA (49,50) and bacterial RecA (51). Therefore, the data suggest that the core ATPase domains of Rad51 and Dmc1 are a common target for Rad54B binding. Notably, when we performed this assay using His_6-tagged Rad54B purified according to the present purification method, which differs from that described previously (39), the same results were observed (data not shown). Hence, our previous result was not related to the His_6-tag fused to the N-terminus of Rad54B. Instead, the difference was probably due to the difference in the purification methods.

To gain further evidence that Rad54B actually interacts with Dmc1, Rad54B and Dmc1 were co-expressed in Sf9 insect cells, and immunoprecipitation was performed. When the cell lysate was mixed with anti-Rad54B antibody-conjugated beads, Dmc1 co-precipitated (Figure 1C, lane 3). Similarly, Rad54B was co-precipitated by anti-Dmc1 antibody-conjugated beads (Figure 1C, lane 6). Therefore, these results demonstrate that Rad54B and Dmc1 can interact in living cells.

Stimulation of the Dmc1-mediated DNA strand exchange by Rad54B

We next examined whether Rad54B affects the DNA strand exchange activity of Dmc1. In this assay, ϕX174 circular ssDNA and homologous linear dsDNA were used as substrates (Figure 2A), and the reactions were conducted in the presence of RPA. Dmc1 was first incubated with ssDNA, and then dsDNA was added into the reaction mixture (standard procedure, Figure 2B, lane 2). A nicked circular duplex is generated when complete strand transfer takes place (Figure 2A). Rad54B itself did not promote strand exchange (Figure 2B, lane 7). When Rad54B was added to the reaction mixture along with the linear dsDNA substrate in the standard procedure, the Dmc1-mediated strand exchange was significantly enhanced (Figure 2B–E). In the experiments presented here, we observed that only sub-stoichiometric amounts of Rad54B (0.025 μM) were required to stimulate the Dmc1-mediated strand exchange (7.5 μM Dmc1). Therefore, Rad54B may act as a trigger in the conversion of the Dmc1–DNA complex from an inactive to an active form.

Rad54B stabilizes the Dmc1–ssDNA complex

Mazin *et al.* (52) demonstrated that Rad51 filaments on ssDNA are stabilized by Rad54, and proposed that this is essential for the stimulation of the Rad51-mediated strand exchange. We therefore investigated whether Rad54B stabilizes the Dmc1–ssDNA complex, by monitoring the transfer of Dmc1 molecules preassembled on ssDNA to a competitor DNA, using two different experimental procedures.

First, we performed a pull down assay using biotinylated DNA and streptavidin beads. In this assay, Dmc1 was assembled on a biotinylated 120mer ssDNA (SAT-120), and was incubated in the presence or absence of Rad54B, followed by the addition of ϕX174 circular ssDNA as a competitor. After SAT-120 was immobilized on the streptavidin beads, the reaction mixture was divided into the beads and the supernatant (Figure 3A). The supernatant was fractionated on a 4–20% gradient SDS–PAGE gel (Figure 3B). When we performed this assay without competitor DNA, there was essentially no Dmc1 detected in the supernatant (data not shown), indicating that Dmc1 was bound to SAT-120. In the presence of competitor DNA, Dmc1 was detectable in the supernatant, indicating that Dmc1 transferred from the preassembled Dmc1–ssDNA complex to the competitor DNA. The amount of Dmc1 transferred in the presence of Rad54B was ~3-fold

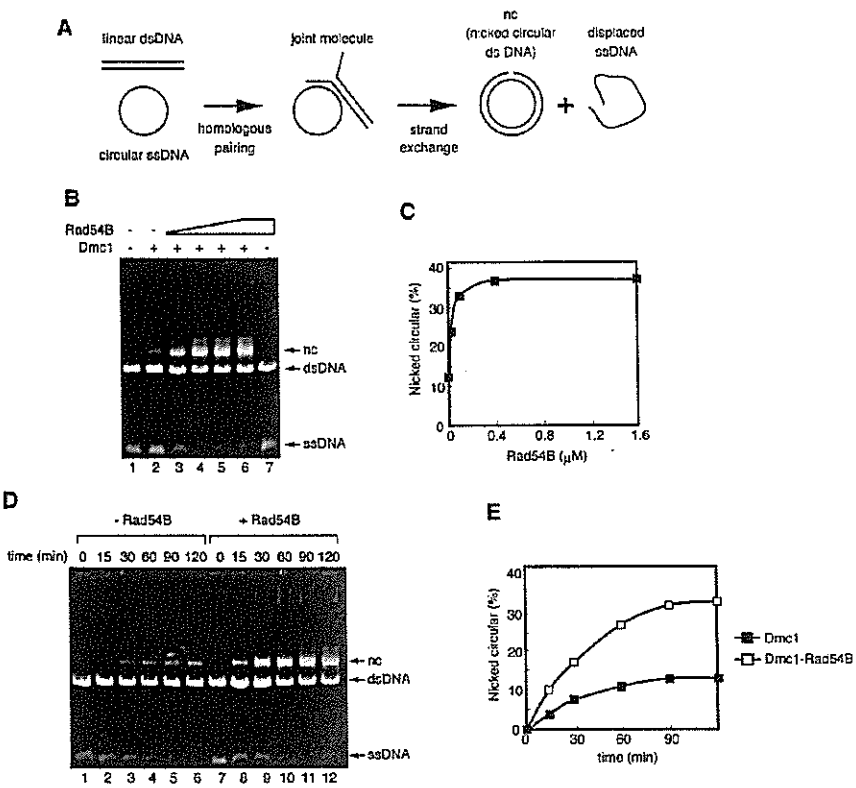

Figure 2. Stimulation of the Dmc1-mediated DNA strand exchange activity by Rad54B. (**A**) Schematic representation of the DNA strand exchange assay. The nucleoprotein filament is formed by incubating Dmc1 with circular ssDNA. The filament is paired with homologous linear dsDNA to yield a joint molecule. A nicked circular duplex (nc) and linear ssDNA are then generated by completing strand exchange over the length of the DNA molecules. (**B**) Dmc1-mediated DNA strand exchange activity with Rad54B. A constant amount of Dmc1 (7.5 μM) was incubated for 2 h with ϕX174 circular ssDNA (30 μM), ϕX174 linear dsDNA (22 μM), RPA (2 μM), KCl (200 mM) and increasing concentrations of Rad54B (0, 0.025, 0.1, 0.4 and 1.6 μM in lanes 2–6, respectively), in the order described for the procedure at 37°C. In lane 1, ssDNA and dsDNA were incubated in buffer with RPA and KCl, but without other recombinant proteins, and in lane 7, ssDNA and dsDNA were incubated in buffer with RPA, KCl and Rad54B (1.6 μM), but no Dmc1. The reaction mixtures were deproteinized, fractionated on a 1% agarose gel and stained with ethidium bromide. (**C**) Graphic representation of the experiments shown in (B). The amounts of nicked circular duplex are presented. (**D**) Time course experiments for DNA strand exchange. Dmc1 (7.5 μM) was incubated with ϕX174 circular ssDNA (30 μM), ϕX174 linear dsDNA (22 μM), RPA (2 μM) and KCl (200 mM), in the presence (open squares) or absence (closed squares) of Rad54B (0.4 μM), in the order described for the procedure at 37°C, for the indicated times. (**E**) Graphic representation of the experiments shown in (D). The amounts of nicked circular duplex are graphically presented.

less than that in the absence of Rad54B (Figure 3C), implying that Rad54B prevented the Dmc1–ssDNA complex from dissociating.

Second, a gel mobility shift assay was carried out to confirm that Rad54B actually stabilizes the Dmc1–ssDNA complex. Dmc1 was assembled on ϕX174 circular ssDNA, and was incubated in the presence or absence of Rad54B, followed by the addition of ϕX174 ssDNA fragments (~500 bases) as a competitor. In this assay, by monitoring the migration distance of the ϕX174 circular ssDNA, we investigated whether the transfer of Dmc1 occurred. In the absence of Rad54B, increasing the concentration of the competitor DNA resulted in the faster mobility of the Dmc1–ssDNA complex on the agarose gel (Figure 4, lanes 2–6). This result indicates that the Dmc1 had transferred from the preassembled Dmc1–ssDNA complex to the competitor DNA. In contrast, in the presence of Rad54B, the migration distances of the Dmc1–ssDNA–Rad54B complexes did not change upon titration with excess amounts of the competitor DNA, indicating that Rad54B inhibited the transfer of Dmc1 from the preassembled complex to the competitor DNA (Figure 4, lanes 7–11). Therefore, Rad54B stabilizes the Dmc1–ssDNA complex.

Rad54B associates with the terminus of the Dmc1–ssDNA helical filament

We next used electron microscopy to examine whether the nature of the Dmc1–ssDNA complex would change by the addition of Rad54B. In both the absence and presence of Rad54B, the Dmc1–ssDNA helical filament was observed (Figure 5A and B). However, in the presence of Rad54B, we observed Dmc1–ssDNA filaments with a mass of ~20 nm associated with the termini (Figure 5C, closed arrow). We did not detect such protein–DNA complexes without Rad54B, implying that Rad54B associated with the terminus of the Dmc1–ssDNA filament. Interestingly, Rad54 preferentially associates with the terminus of the

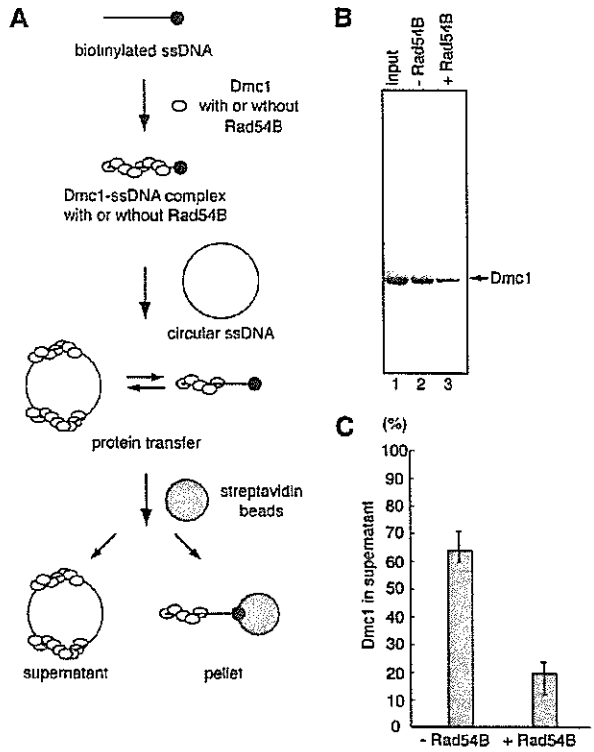

Figure 3. Pull down assay for the protein transfer between ssDNA molecules. (A) A schematic diagram of the pull down assay. Dmc1 and biotinylated DNA form a complex in the absence or presence of Rad54B. Then, circular ssDNA is added as a competitor, and protein transfer occurs. Biotinylated DNA is immobilized on streptavidin beads, and the reaction mixture is divided into the beads and supernatant. (B) Dmc1 (5 μM) was incubated with SAT-120 (20 μM) labeled with biotin at the 5′ end in the absence (lane 2) or presence (lane 3) of Rad54B (200 nM), followed by an incubation with ϕX174 circular ssDNA (2 mM). After immobilization on streptavidin beads for 1 h at 4°C, the reaction mixture was divided into the beads and the supernatant by centrifugation. Then, one-tenth of the supernatant was fractionated on a 4–20% gradient SDS–PAGE gel. Lane 1 is one-tenth of the input protein. (C) Graphic representation of the experiments shown in (B). The amounts of Dmc1 within the supernatant are presented.

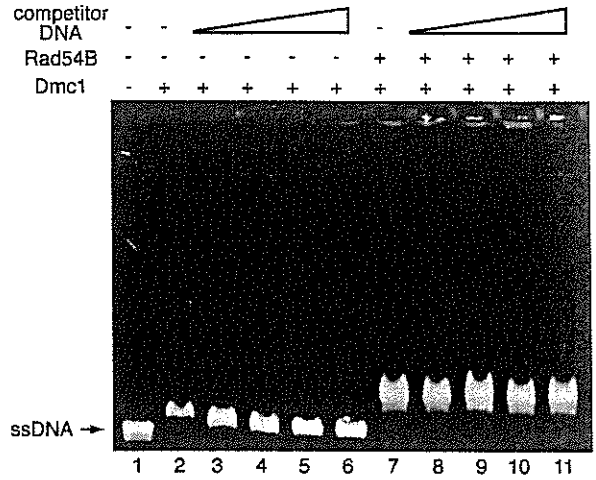

Figure 4. Gel mobility shift assay for the protein transfer between ssDNA molecules. A constant amount of Dmc1 (10 μM) was incubated with ϕX174 circular ssDNA (20 μM) in the absence (lanes 2–6) or presence (lanes 7–11) of Rad54B (200 nM), followed by an incubation with increasing amounts of ϕX174 ssDNA fragments (0, 25, 50, 100 and 200 μM in lanes 2–6 and lanes 7–11, respectively) at 37°C for 2 h. In lane 1, ϕX174 circular ssDNA was incubated in buffer without any recombinant proteins.

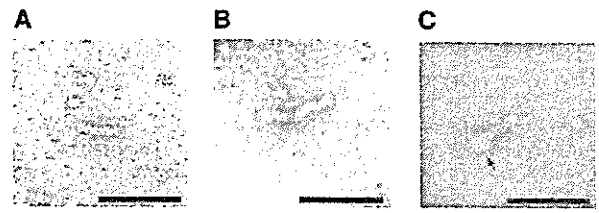

Figure 5. Electron microscopic images of Rad54B and Dmc1 with ssDNA. Images of the Dmc1–ssDNA helical filament in the absence (A) or presence (B) of Rad54B, and the Rad54B–Dmc1–ssDNA complex (C) were photographed after negative staining with uranyl acetate. The closed bar denotes 100 nm.

Rad51–dsDNA helical filament (53). This terminal association of Rad54B may stabilize the Dmc1–ssDNA filament.

DISCUSSION

The yeast and human Rad54 proteins stimulate strand exchange by Rad51 (54,55), but, thus far, the activation of Dmc1-mediated strand exchange by the Rad54 homologs has not been reported. The present findings suggest that the human Rad54B protein stimulates the Dmc1-mediated strand exchange, probably through the stabilization of the presynaptic filament formed by ssDNA and Dmc1. Recent studies have shown that Rad54B enhances D-loop formation by Dmc1 and Rad51 (22,38). Taken together, Rad54B assists Dmc1 in the initial strand invasion step (homologous pairing), as well as in the extension of the heteroduplex region (strand exchange). To stabilize the Dmc1–ssDNA complex, catalytic amounts of Rad54B were sufficient. Consistent with this result, we observed that Rad54B associated with the termini of the Dmc1–ssDNA filament, by an electron microscopic analysis. These observations suggest that Rad54B may stabilize the Dmc1–ssDNA complex by interacting with the terminal region of the Dmc1–ssDNA complex.

How could Rad54B stabilize the Dmc1–ssDNA complexes? One possibility is that Rad54B could prevent the Dmc1–ssDNA nucleoprotein filament from disassembling by binding to one end of the filament. This may lead to the unidirectional assembly of the Dmc1–ssDNA nucleoprotein filament at the DSB site. The second possibility is that by physically interacting with Dmc1, Rad54B could alter the conformation of the Dmc1–ssDNA nucleoprotein filament from an inactive form to an active form. Multiple studies have indicated that the fundamental mechanism of Dmc1-mediated recombination is the same as that of the RecA homologs, suggesting that Dmc1 forms helical filaments when

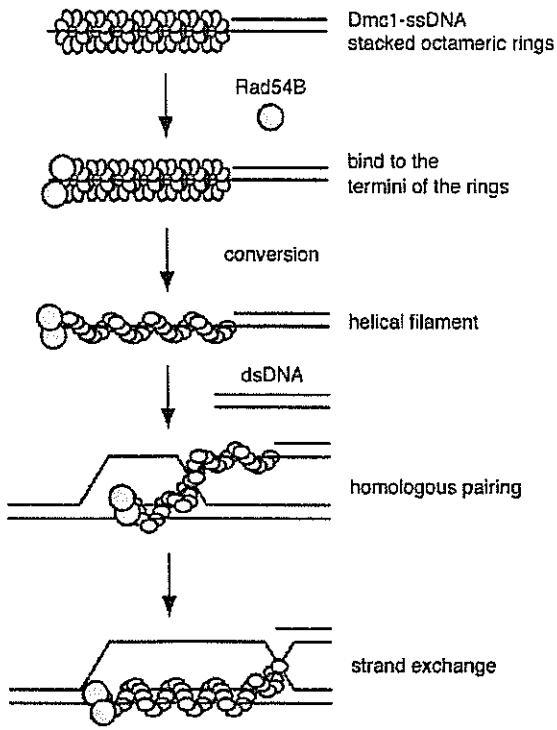

Figure 6. Model of Rad54B converting the Dmc1–DNA complex from the octameric ring form to the helical filament form. Rad54B interacts with terminus of the stacked octameric rings of the Dmc1–DNA complex, causing a conversion into the helical-filament form. This conversion results in the stabilization of the Dmc1–ssDNA complex, and the stimulation of the DNA strand exchange promoted by Dmc1.

performing the strand exchange reaction (22,45,48,56–58). However, Dmc1 forms octameric rings alone and on DNA (59), and the conversion from rings to filaments is probably essential for the proper function of Dmc1. A recent study indicated that ATP binding may act as a trigger in the conversion of the Dmc1 octameric ring form to the helical filament form (43). We found that Rad54B bound to the isolated ATPase domain of Dmc1, and this interaction may assist in changing in the conformation of the Dmc1 monomer to favor the formation of the helical filament, thus stabilizing the complex. Based on these possibilities, we propose the following model (Figure 6), which explains the mechanism of DNA strand exchange promoted by Rad54B and Dmc1. First, Rad54B associates with the terminus of the stacked rings, and binds to the ATPase domain of Dmc1. This process may catalytically prevent the Dmc1–ssDNA filament from disassembling or promote the conversion of the Dmc1–DNA complex from stacked octameric rings to helical filaments. The Dmc1–ssDNA nucleoprotein filament, which is probably the active form for the strand exchange reaction, then invades the homologous duplex DNA, forming a heteroduplex DNA intermediate.

Recent studies have shown that Rad54 has a potent translocase activity and stimulates the branch migration activity of Rad51 (55,60). These activities suggest that Rad54 is involved in the post-synaptic phase of recombination. Although the previous and present Rad54B results have suggested its involvement in the presynaptic phase of recombination, it is easy to imagine that Rad54B functions in the post-synaptic phase of recombination, such as Rad54. Further analyses of the effects of Rad54B on Dmc1 complexed with various DNA structures representing recombination intermediates may provide clues toward understanding the precise mechanism of the Rad54B-stimulated homologous recombination.

ACKNOWLEDGEMENTS

We thank R. Enomoto (RIKEN GSC), Y. Takizawa (Waseda University) and N. Nagashima (Waseda University) for technical assistance. This work was supported by the RIKEN Structural Genomics/Proteomics Initiative (RSGI), the National Project on Protein Structural and Functional Analyses, and Grants-in-Aid from the Japanese Society for the Promotion of Science (JSPS) and the Ministry of Education, Sports, Culture, Science, and Technology, Japan. Funding to pay the Open Access publication charges for this article was provided by RIKEN Genomic Sciences Center.

Conflict of interest statement. None declared.

REFERENCES

1. Whitaker,S.J. (1992) DNA damage by drugs and radiation: what is important and how is it measured? *Eur. J. Cancer*, **28**, 273–276.
2. Cox,M.M., Goodman,M.F., Kreuzer,K.N., Sherratt,D.J., Sandler,S.J. and Marians,K.J. (2000) The importance of repairing stalled replication forks. *Nature*, **404**, 37–41.
3. Ward,J.F. (1994) The complexity of DNA damage: relevance to biological consequences. *Int. J. Radiat. Biol.*, **66**, 427–432.
4. Caldecott,K.W. (2001) Mammalian DNA single-strand break repair: an X-ra(y)ted affair. *Bioessays*, **23**, 447–455.
5. Kleckner,N. (1996) Meiosis: how could it work? *Proc. Natl Acad. Sci. USA*, **93**, 8167–8174.
6. Keeney,S., Gitoux,C.N. and Kleckner,N. (1997) Meiosis-specific DNA double-strand breaks are catalyzed by Spo11, a member of a widely conserved protein family. *Cell*, **88**, 375–384.
7. Shibata,T., DasGupta,C., Cunningham,R.P. and Radding,C.M. (1979) Purified *Escherichia coli* recA protein catalyzes homologous pairing of superhelical DNA and single-stranded fragments. *Proc. Natl Acad. Sci. USA*, **76**, 1638–1642.
8. McEntee,K., Weinstock,G.M. and Lehman,I.R. (1979) Initiation of general recombination catalyzed *in vitro* by the recA protein of *Escherichia coli*. *Proc. Natl Acad. Sci. USA*, **76**, 2615–2619.
9. Cox,M.M. and Lehman,I.R. (1981) recA protein of *Escherichia coli* promotes branch migration, a kinetically distinct phase of DNA strand exchange. *Proc. Natl Acad. Sci. USA*, **78**, 3433–3437.
10. Cox,M.M. and Lehman,I.R. (1981) Directionality and polarity in recA protein-promoted branch migration. *Proc. Natl Acad. Sci. USA*, **78**, 6018–6022.
11. West,S.C., Cassuto,E. and Howard-Flanders,P. (1981) recA protein promotes homologous-pairing and strand-exchange reactions between duplex DNA molecules. *Proc. Natl Acad. Sci. USA*, **78**, 2100–2104.
12. Howard-Flanders,P., West,S.C. and Stasiak,A. (1984) Role of RecA protein spiral filaments in genetic recombination. *Nature*, **309**, 215–219.
13. Bishop,D.K., Park,D., Xu,L. and Kleckner,N. (1992) DMC1: a meiosis-specific yeast homolog of *E.coli* recA required for recombination, synaptonemal complex formation, and cell cycle progression. *Cell*, **69**, 439–456.
14. Shinohara,A., Ogawa,H. and Ogawa,T. (1992) Rad51 protein involved in repair and recombination in *S.cerevisiae* is a RecA-like protein. *Cell*, **69**, 457–470.

15. Shinohara,A., Ogawa,H., Matsuda,Y., Ushio,N., Ikeo,K. and Ogawa,T. (1993) Cloning of human, mouse and fission yeast recombination genes homologous to RAD51 and recA. *Nature Genet.*, **4**, 239–243.
16. Habu,T., Taki,T., West,A., Nishimune,Y. and Morita,T. (1996) The mouse and human homologs of DMC1, the yeast meiosis-specific homologous recombination gene, have a common unique form of exon-skipped transcript in meiosis. *Nucleic Acids Res.*, **24**, 470–477.
17. Sung,P. (1994) Catalysis of ATP-dependent homologous DNA pairing and strand exchange by yeast RAD51 protein. *Science*, **265**, 1241–1243.
18. Baumann,P., Benson,F.E. and West,S.C. (1996) Human Rad51 protein promotes ATP-dependent homologous pairing and strand transfer reactions *in vitro*. *Cell*, **87**, 757–766.
19. Gupta,R.C., Bazemore,L.R., Golub,E.I. and Radding,C.M. (1997) Activities of human recombination protein Rad51. *Proc. Natl Acad. Sci. USA*, **94**, 463–468.
20. Li,Z., Golub,E.I., Gupta,R. and Radding,C.M. (1997) Recombination activities of HsDmc1 protein, the meiotic human homolog of RecA protein. *Proc. Natl Acad. Sci. USA*, **94**, 11221–11226.
21. Hong,E.L., Shinohara,A. and Bishop,D.K. (2001) *Saccharomyces cerevisiae* Dmc1 protein promotes renaturation of single-strand DNA (ssDNA) and assimilation of ssDNA into homologous super-coiled duplex DNA. *J. Biol. Chem.*, **276**, 41906–41912.
22. Sehorn,M.G., Sigurdsson,S., Bussen,W., Unger,V.M. and Sung,P. (2004) Human meiotic recombinase Dmc1 promotes ATP-dependent homologous DNA strand exchange. *Nature*, **429**, 433–437.
23. Symington,L.S. (2002) Role of RAD52 epistasis group genes in homologous recombination and double-strand break repair. *Microbiol. Mol. Biol. Rev.*, **66**, 630–670.
24. Sung,P., Krejci,L., Van Komen,S. and Sehorn,M.G. (2003) Rad51 recombinase and recombination mediators. *J. Biol. Chem.*, **278**, 42729–42732.
25. Eisen,J.A., Sweder,K.S. and Hanawalt,P.C. (1995) Evolution of the SNF2 family of proteins: subfamilies with distinct sequences and functions. *Nucleic Acids Res.*, **23**, 2715–2723.
26. Swagemakers,S.M., Essers,J., de Wit,J., Hoeijmakers,J.H. and Kanaar,R. (1998) The human RAD54 recombinational DNA repair protein is a double-stranded DNA-dependent ATPase. *J. Biol. Chem.*, **273**, 28292–28297.
27. Alexiadis,V. and Kadonaga,J.T. (2002) Strand pairing by Rad54 and Rad51 is enhanced by chromatin. *Genes Dev.*, **16**, 2767–2771.
28. Alexeev,A., Mazin,A. and Kowalczykowski,S.C. (2003) Rad54 protein possesses chromatin-remodeling activity stimulated by the Rad51–ssDNA nucleoprotein filament. *Nature Struct. Biol.*, **10**, 182–186.
29. Jaskelioff,M., Van Komen,S., Krebs,J.E., Sung,P. and Peterson,C.L. (2003) Rad54p is a chromatin remodeling enzyme required for heteroduplex DNA joint formation with chromatin. *J. Biol. Chem.*, **278**, 9212–9218.
30. Wolner,B. and Peterson,C.L. (2005) ATP-dependent and ATP-independent roles for the Rad54 chromatin remodeling enzyme during recombinational repair of a DNA double strand break. *J. Biol. Chem.*, **280**, 10855–10860.
31. Alexiadis,V., Lusser,A. and Kadonaga,J.T. (2004) A conserved N-terminal motif in Rad54 is important for chromatin remodeling and homologous strand pairing. *J. Biol. Chem.*, **279**, 27824–27829.
32. Essers,J., Hendriks,R.W., Swagemakers,S.M., Troelstra,C., de Wit,J., Bootsma,D., Hoeijmakers,J.H. and Kanaar,R. (1997) Disruption of mouse RAD54 reduces ionizing radiation resistance and homologous recombination. *Cell*, **89**, 195–204.
33. Tan,T.L., Essers,J., Citterio,E., Swagemakers,S.M., de Wit,J., Benson,F.E., Hoeijmakers,J.H. and Kanaar,R. (1999) Mouse Rad54 affects DNA conformation and DNA-damage-induced Rad51 foci formation. *Curr. Biol.*, **9**, 325–328.
34. Van Komen,S., Petukhova,G., Sigurdsson,S., Stratton,S. and Sung,P. (2000) Superhelicity-driven homologous DNA pairing by yeast recombination factors Rad51 and Rad54. *Mol. Cell*, **6**, 563–572.
35. Petukhova,G., Stratton,S. and Sung,P. (1998) Catalysis of homologous DNA pairing by yeast Rad51 and Rad54 proteins. *Nature*, **393**, 91–94.
36. Sigurdsson,S., Van Komen,S., Petukhova,G. and Sung,P. (2002) Homologous DNA pairing by human recombination factors Rad51 and Rad54. *J. Biol. Chem.*, **277**, 42790–42794.
37. Solinger,J.A., Kiianitsa,K. and Heyer,W.D. (2002) Rad54, a Swi2/Snf2-like recombinational repair protein, disassembles Rad51:dsDNA filaments. *Mol. Cell*, **10**, 1175–1188.
38. Wesoly,J., Agarwal,S., Sigurdsson,S., Bussen,W., Van Komen,S., Qin,J., Van Steeg,H., Van Benthem,J., Wassenaar,E., Baarends,W.M. *et al.* (2006) Differential contributions of mammalian Rad54 paralogs to recombination, DNA damage repair, and meiosis. *Mol. Cell. Biol.*, **26**, 976–989.
39. Tanaka,K., Kagawa,W., Kinebuchi,T., Kurumizaka,H. and Miyagawa,K. (2002) Human Rad54B is a double-stranded DNA-dependent ATPase and has biochemical properties different from its structural homolog in yeast, Tid1/Rdh54. *Nucleic Acids Res.*, **30**, 1346–53.
40. Hiramoto,T., Nakanishi,T., Sumiyoshi,T., Fukuda,T., Matsuura,S., Tauchi,H., Komatsu,K., Shibasaki,Y., Inui,H., Watatani,M. *et al.* (1999) Mutation of a novel human RAD54 homologue, RAD54B, in primary cancer. *Oncogene*, **18**, 3422–3426.
41. Miyagawa,K., Tsuruga,T., Kinomura,A., Usui,K., Katsura,M., Tashiro,S., Mishima,H. and Tanaka,K. (2002) A role for RAD54B in homologous recombination in human cells. *EMBO J.*, **21**, 175–180.
42. Kagawa,W., Kurumizaka,H., Ikawa,S., Yokoyama,S. and Shibata,T. (2001) Homologous pairing promoted by the human Rad52 protein. *J. Biol. Chem.*, **276**, 35201–35208.
43. Kinebuchi,T., Kagawa,W., Enomoto,R., Tanaka,K., Miyagawa,K., Shibata,T., Kurumizaka,H. and Yokoyama,S. (2004) Structural basis for octameric ring formation and DNA interaction of the human homologous-pairing protein Dmc1. *Mol. Cell*, **14**, 363–374.
44. Henricksen,L.A., Umbricht,C.B. and Wold,M.S. (1994) Recombinant replication protein A: expression, complex formation, and functional characterization. *J. Biol. Chem.*, **269**, 11121–11132.
45. Kinebuchi,T., Kagawa,W., Kurumizaka,H. and Yokoyama,S. (2005) Role of the N-terminal domain of the human DMC1 protein in octamer formation and DNA binding. *J. Biol. Chem.*, **280**, 28382–28387.
46. Tanaka,K., Hiramoto,T., Fukuda,T. and Miyagawa,K. (2000) A novel human rad54 homologue, Rad54B, associates with Rad51. *J. Biol. Chem.*, **275**, 26316–26321.
47. Pellegrini,L., Yu,D.S., Lo,T., Anand,S., Lee,M., Blundell,T.L. and Venkitaraman,A.R. (2002) Insights into DNA recombination from the structure of a RAD51–BRCA2 complex. *Nature*, **420**, 287–293.
48. Conway,A.B., Lynch,T.W., Zhang,Y., Fortin,G.S., Fung,C.W., Symington,L.S. and Rice,P.A. (2004) Crystal structure of a Rad51 filament. *Nature Struct. Mol. Biol.*, **11**, 791–796.
49. Shin,D.S., Pellegrini,L., Daniels,D.S., Yelent,B., Craig,L., Bates,D., Yu,D.S., Shivji,M.K., Hitomi,C., Arvai,A.S. *et al.* (2003) Full-length archaeal Rad51 structure and mutants: mechanisms for RAD51 assembly and control by BRCA2. *EMBO J.*, **22**, 4566–4576.
50. Wu,Y., He,Y., Moya,I.A., Qian,X. and Luo,Y. (2004) Crystal structure of archaeal recombinase RADA: a snapshot of its extended conformation. *Mol. Cell*, **15**, 423–435.
51. Story,R.M., Weber,I.T. and Steitz,T.A. (1992) The structure of the *E. coli* recA protein monomer and polymer. *Nature*, **355**, 318–325.
52. Mazin,A.V., Alexeev,A.A. and Kowalczykowski,S.C. (2003) A novel function of Rad54 protein. Stabilization of the Rad51 nucleoprotein filament. *J. Biol. Chem.*, **278**, 14029–14036.
53. Kiianitsa,K., Solinger,J.A. and Heyer,W.D. (2006) Terminal association of Rad54 protein with the Rad51–dsDNA filament. *Proc. Natl Acad. Sci. USA*, **103**, 9767–9772.
54. Solinger,J.A., Lutz,G., Sugiyama,T., Kowalczykowski,S.C. and Heyer,W.D. (2001) Rad54 protein stimulates heteroduplex DNA formation in the synaptic phase of DNA strand exchange via specific interactions with the presynaptic Rad51 nucleoprotein filament. *J. Mol. Biol.*, **307**, 1207–1221.
55. Bugreev,D.V., Mazina,O.M. and Mazin,A.V. (2006) Rad54 protein promotes branch migration of Holliday junction. *Nature*, **442**, 590–593.
56. Gupta,R.C., Golub,E., Bi,B. and Radding,C.M. (2001) The synaptic activity of HsDmc1, a human recombination protein specific to meiosos. *Proc. Natl Acad. Sci. USA*, **98**, 8433–8439.

57. Bugreev,D.V., Golub,E.I., Stasiak,A.Z., Stasiak,A. and Mazin,A.V. (2005) Activation of human meiosis-specific recombinase Dmc1 by Ca^{2+}. *J. Biol. Chem.*, **280**, 26886–26895.
58. Sauvageau,S., Stasiak,A.Z., Banville,I., Ploquin,M., Stasiak,A. and Mason,J.Y. (2005) Fission yeast rad51 and dmc1, two efficient DNA recombinases forming helical nucleoprotein filaments. *Mol. Cell. Biol.*, **25**, 4377–4387.
59. Passy,S.I., Yu,X., Li,Z., Radding,C.M., Masson,J.Y., West,S.C. and Egelman,E.H. (1999) Human Dmc1 protein binds DNA as an octameric ring. *Proc. Natl Acad. Sci. USA*, **96**, 10684–10688.
60. Amitani,I., Baskin,R.J. and Kowalczykowski,S.C. (2006) Visualization of Rad54, a chromatin remodeling protein, translocating on single DNA molecules. *Mol. Cell*, **23**, 143–148.

Available online at www.sciencedirect.com
ScienceDirect
Biochemical and Biophysical Research Communications 348 (2006) 728–734
BBRC
www.elsevier.com/locate/ybbrc

Suppression of anchorage-independent growth by expression of the ataxia-telangiectasia group D complementing gene, *ATDC*

Yoshio Hosoi [a,b,*], Leon N. Kapp [b], John P. Murnane [b,c], Yoshihisa Matsumoto [a], Atsushi Enomoto [a], Tetsuya Ono [d], Kiyoshi Miyagawa [a]

[a] *Department of Radiation Research, Faculty of Medicine, University of Tokyo, Tokyo 113-0033, Japan*
[b] *Laboratory of Radiobiology and Environmental Health, University of California, San Francisco, San Francisco, CA 94103, USA*
[c] *Radiation Oncology Research Laboratory, University of California, San Francisco, San Francisco, CA 94103, USA*
[d] *Department of Radiation Research, Tohoku University School of Medicine, Sendai 980-8575, Japan*

Received 19 July 2006
Available online 28 July 2006

Abstract

The ataxia-telangiectasia group D complementing gene, *ATDC*, is located at 11q23, where loss of heterozygosity (LOH) is frequently observed in many kinds of cancers including breast cancer. Underexpression of *ATDC* in breast and prostate cancer has been reported using serial analysis of gene expression (SAGE) and DNA microarray analysis. We previously reported that SV-40-transformation down-regulates the expression of *ATDC*. In the present study, we investigated the roles of *ATDC* in carcinogenesis. First, we investigated the expression of *ATDC* in 11 cancer cell lines. No detectable transcript was observed in 4 tumor cell lines, and no ATDC protein was detected in 8 tumor cell lines. We transfected *ATDC* expression vector into Saos-2 and BT-549 that lacked detectable mRNA and protein expression of *ATDC*. Colony-forming efficiency in soft agar was significantly suppressed in all of the *ATDC* transfectants. These results suggest that suppressed *ATDC* expression is associated with malignant phenotype.

Keywords: *ATDC*; LOH; 11q23; Suppressor oncogene; Carcinogenesis; Transformation

A candidate gene for ataxia-telangiectasia (AT) group D (*ATDC*) has been cloned in 1992 [1]. AT is an autosomal recessive human genetic disease characterized by immunological deficiencies, neurological degeneration, developmental abnormalities, and an increased risk of cancer [2]. Cells from AT patients show hyper-sensitivity to ionizing radiation, radioresistant DNA synthesis, elevated recombination, cell cycle abnormalities, and aberrant cytoskeletal organization [2]. *ATDC* partially restores resistance to ionizing radiation in cells derived from AT patients, although it does not affect radioresistant DNA synthesis [3]. The *ATDC* gene is located at 11q23 and is closely linked to THY1 and D11S528 [1]. *ATDC* is likely to be a member of a gene family whose proteins are characterized by zinc finger and leucine zipper motifs [4]. Recently ATDC has been reported to be a member of tripartite motif (TRIM) protein family, which is characterized by three zinc-binding domains, a RING, a B-box type 1, and a B-box type 2, followed by a coiled-coil region [5–7]. The ATDC protein physically interacts with the intermediate-filament protein vimentin, which is a protein kinase C substrate, and with hPKCI-1, which is an inhibitor of protein kinase C [8,9].

We previously reported that SV-40-transformation affects the expression of *ATDC* [10]. Because the large T antigen of SV-40 binds with the products of suppressor oncogenes such as *p53* and the retinoblastoma gene (*RB*) [11,12], the downregulation of *ATDC* expression, and the change in the splicing pattern observed in SV-40-transformed cells might have relevance to cellular transformation [10]. Furthermore, high frequencies of loss of

* Corresponding author. Fax: +81 3 5841 3013.
E-mail address: hosoi@m.u-tokyo.ac.jp (Y. Hosoi).

0006-291X/$ - see front matter © 2006 Elsevier Inc. All rights reserved.
doi:10.1016/j.bbrc.2006.07.115

heterozygosity (LOH) at 11q23, where *ATDC* is located, have been observed in various malignancies, including breast cancer [13]. In addition, underexpression of *ATDC* in breast and prostate cancer has been reported using serial analysis of gene expression (SAGE) and DNA microarray analysis [14,15]. These reports indicate that *ATDC* might have relevance to carcinogenesis.

In the present study, we examined expression of *ATDC* using 11 tumor cell lines. No *ATDC* transcripts were observed in 4 tumor cell lines by Northern blot analysis, no ATDC protein was detected in 8 tumor cell lines by Western blot analysis. Transfection of *ATDC* into two tumor cell lines lacking detectable mRNA and protein expression of *ATDC* resulted in suppression of colony-forming efficiency in soft agar, which suggests that suppressed *ATDC* expression is associated with the malignant phenotype in these tumor cell lines.

Materials and methods

Cell lines. LM217 is an SV-40-transformed cell line derived from human fibroblast cells HS27 [16]. We obtained the following 11 cancer cell lines from American Type Culture Collection (Manassas, VA): a fibrosarcoma cell line HT-1080, a transitional cell carcinoma cell line T24, an osteosarcoma cell line Saos-2, breast cancer cell lines BT-549, MDA-MB-231, MDA-MB-436, MDA-MB-468, SK-BR-3, and MDA-MB-453, and retinoblastoma cell lines Y79 and WERI-Rb-1.

Northern blot analysis. mRNA was prepared using Fast Track mRNA isolation kits (Invitrogen, Carlsbad, CA). RNA gel electrophoresis and RNA blot analysis were carried out using standard procedures. Ten micrograms of mRNA was applied to each lane of the Northern blots, and the blots were probed using the 3.0 kbp transcript of *ATDC* [1]. For detection of 18S and 28S ribosomal RNA, gels were stained with ethidium bromide and illuminated with UV radiation before hybridization.

Western blot analysis. Cells were lysed in the electrophoresis sample buffer (62.5 mM Tris, pH 6.8; 2% SDS; 5% glycerol; 0.003% bromophenol blue; 1% β-mercaptoethanol) and boiled for 5 min. The cell lysate was resolved by 10% polyacrylamide gel electrophoresis and was electrophoretically transferred to polyvinylidene difluoride membranes (Millipore Corporation, Bedford, MA). Whole cell lysate prepared from 10^5 cells for detection of ATDC protein or 3×10^3 cells for detection of β-actin protein was loaded in each lane. The membranes were then probed with anti-ATDC antibody N-19 (Santa Cruz Biotechnology, Inc., Santa Cruz, CA) or anti-β-actin antibody AC-15 (SIGMA, Saint Louis, MO). The antigen-antibody complexes were detected by the ECL Plus™ Western blotting detection reagents (Amersham Pharmacia Biotech Inc., Piscataway, NJ) using horseradish peroxidase-conjugated antibodies.

Construction of a 3.0 kbp ATDC expression vector. The *ATDC* cDNA was isolated from a commercially available library contained within a λ ZAPII vector (Stratagene, La Jolla, CA) as previously described [1]. The cDNA was rescued from ZAPII and cloned into the Bluescript plasmid (Stratagene) [4]. The *ATDC* expression vector, pcD2E-1Bd, was constructed by ligating the *ATDC* cDNA into a mammalian expression vector, pcD2E, which contained the SV-40 promoter and neomycin-/ampicillin-resistant sequences [17]. The expression vector pcD2E was obtained from Dr. C. A. Weber.

Stable transfection in Saos-2 and BT-549 cells. The *ATDC*-containing plasmid pcD2E-1Bd and the control plasmid pcD2E(−) were transfected by the calcium phosphate method. Exponentially growing cells were subcultured onto 100-mm tissue culture dishes and incubated overnight at 35 °C in a 5% CO_2 incubator. Twenty micrograms of plasmid DNA per dish mixed with 0.5 ml of 0.25 M $CaCl_2$ and 0.5 ml of 2× BES-buffered saline (50 mM BES (*N,N*-bis[2-hydroxyethyl]-2-aminoethanesulfonic acid), 280 mM NaCl, and 1.5 mM $NaHPO_4 \cdot 2H_2O$) was added to the dishes, and cells were incubated for 24 h at 35 °C in a 3% CO_2 incubator. After a 24 h incubation, the medium was removed and the cells were rinsed twice with phosphate-buffered saline (PBS). Cells were incubated in fresh medium for 24 h at 37 °C in a 5% CO_2 incubator. The cells were replated and incubated for 24 h at 37 °C in a 5% CO_2 incubator. After a 24 h incubation, the medium was changed to the selective medium containing 400 μg/ml G418 (LIFE TECHNOLOGIES, Rockville, MD). After 2–4 weeks, several colonies were observed in each dish, and each of the G418-resistant colonies was transferred separately to an individual well of 24-well plates. Cells were subsequently maintained in G418 medium.

Reverse transcription-polymerase chain reaction (RT-PCR). Total RNA was prepared using RNA STAT-60™ (TEL-TEST, Friendswood, TX). Two micrograms of mRNA was reverse-transcribed with random hexamer oligonucleotides (Amersham Pharmacia Biotech, Uppsala, Sweden) to produce cDNAs. One-twentieth of each product was used for amplification. PCR for amplification of *ATDC* or β-actin mRNA had 35 cycles or 25 cycles, respectively. Primers used for amplification of *ATDC* mRNA were as follows: 5′ GGAGAAGCAAAAGGAGGAAGTG 3′ (sense); and 5′ TTGGGGCTTTGGCTCCGCATGA 3′ (antisense). The expected size of the product is 699 bp. Primers used for amplification of β-actin mRNA were as follows: 5′ AAGAGAGGCATCCTCACCCT 3′ (sense); and 5′ TACATGGCTGGGGTGTTGAA 3′ (antisense). The expected size of the product is 218 bp.

Colony-forming efficiency in soft agar. Colony-forming efficiency was determined using a double-layer soft-agar method. In 60-mm tissue culture dishes, 10^2–10^5 cells were plated in 0.3% agar over a layer of 0.5% agar. Cells were incubated for 56 days in a CO_2 incubator and colonies that consisted of more than 50 cells were counted.

Cell proliferation rate. One hundred thousand Saos-2 cells or BT-549 cells were plated in 60-mm tissue culture dishes. Saos-2 cells were treated with 0.25% trypsin and 0.1% EDTA 2, 4, 6 or 8 days after subculturing, and BT-549 cells were treated with them 1, 2, 3 or 4 days after subculturing. Total cell number per dish was counted using the COULTER COUNTER MODEL ZBI (Coulter Electronics, Inc., Hialeah, FL), and the proliferation rate was calculated.

Results

mRNA expression of ATDC in cancer cell lines and a SV-40-transformed cell line

First, we examined mRNA expression of *ATDC* in 11 cultured cancer cell lines and a fibroblast cell line (Fig. 1A). Multiple transcripts were observed in LM217, MDA-MB-436, MDA-MB-468, SK-BR-3, and MDA-MB-453. The transcripts consisted chiefly of 3.0, 2.4, and 1.6 kbp mRNA. No transcript was observed in HT-1080, Saos-2, BT-549, Y79, and WERI-Rb-1 in the Northern blots shown in Fig. 1A. A 2.4 kbp transcript could be observed in HT-1080 after long exposure, however, no transcript was observed in Saos-2, BT-549, Y79, and WERI-Rb-1 even after long exposure (data not shown).

Protein expression of ATDC in cancer cell lines and a SV-40-transformed cell line

ATDC protein expression was investigated using the same cell lines. ATDC protein was detected as a band having a molecular weight of approximately 65 kDa in MDA-MB-436, MDA-MB-468, and SK-BR-3 cell lines (Fig. 1B). Molecular weight of 65 kDa is the expected size for a protein predicted to have 588 amino acid residues coded in the

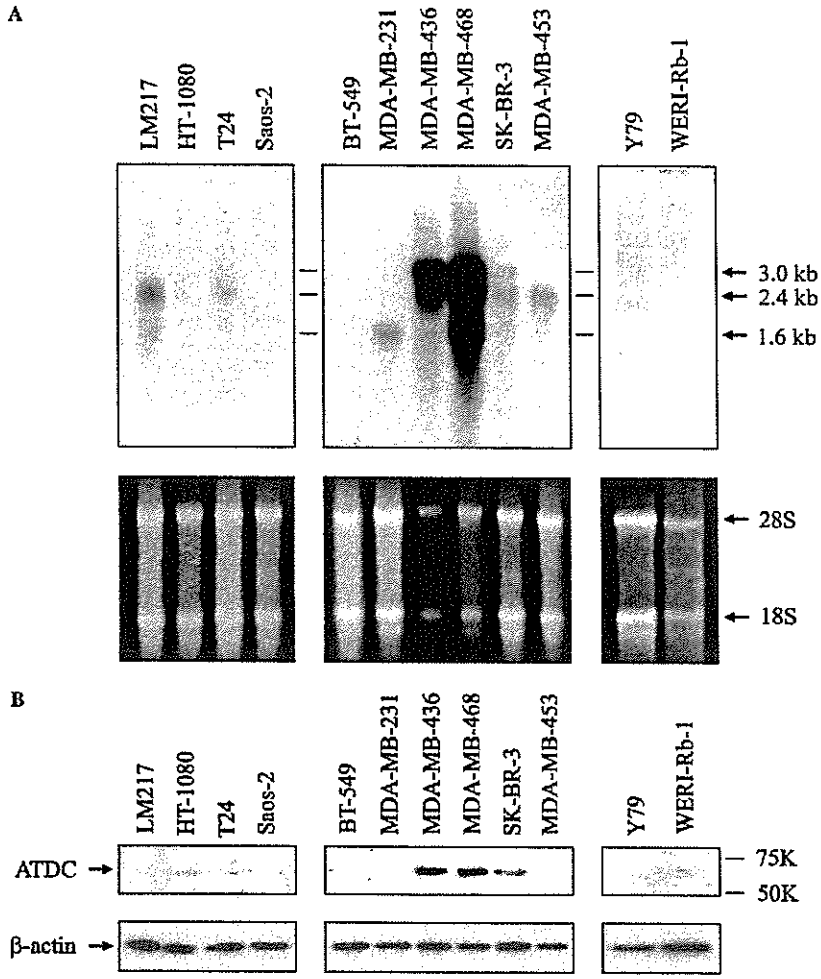

Fig. 1. Northern blot analysis and Western blot analysis of 11 cancer cell lines and a fibroblast cell line. (A) Upper panels show Northern blot analysis probed with the 3.0 kbp *ATDC* cDNA. Ten micrograms of mRNA from normal fibroblast LM217, fibrosarcoma HT-1080, transitional cell carcinoma T24, osteosarcoma Saos-2, breast cancer BT-549, MDA-MB-231, MDA-MB-436, MDA-MB-468, SK-BR-3, and MDA-MB-453, and retinoblastoma Y79 and WERI-Rb-1 was loaded. Lower panels show RNA preparations prior to blotting. (B) ATDC and β-actin proteins were detected by Western blot analysis using anti-ATDC antibody N-19 or anti-β-actin antibody AC-15. Molecular weight of 65 kDa is the expected size for the ATDC protein.

3.0 kbp transcript [4,9]. No band was observed in LM217, HT-1080, T24, Saos-2, BT-549, MDA-MB-231, MDA-MB-453, Y79, and WERI-Rb-1 (Fig. 1B). LM217, HT-1080, T24, MDA-MB-231, and MDA-MB-453 had 2.4 and/or 1.6 kbp transcript, but no ATDC protein was detected in these cell lines (Fig. 1B). Anti-ATDC antibody N-19 used in the present study is a polyclonal antibody raised against a peptide mapping at the amino terminus of the ATDC protein coded in 3.0 kbp transcript. In an attempt to detect ATDC protein coded in 2.4 or 1.6 kbp transcript, we used anti-ATDC antibody C-17 which is a polyclonal antibody raised against a peptide mapping at the carboxy terminus (Santa Cruz Biotechnology, Inc., Santa Cruz, CA). However, no ATDC protein was detected on Western blot with C-17 antibody in these cell lines (data not shown).

Stable transfection of ATDC expression vector in Saos-2 and BT-549

Next, in order to elucidate the roles of *ATDC* gene in carcinogenesis, we transfected the *ATDC* expression vector pcD2E-1Bd or the control vector pcD2E(−) into Saos-2 and BT-549 which lacked detectable *ATDC* expression. We chose Saos-2 and BT-549 for *ATDC* transfection because Y79 and WERI-Rb-1 grew in suspension and it was difficult to get stable transfectants of the gene. We selected randomly 5 clones each from the Saos-2 or BT-549 cells transfected with pcD2E-1Bd or pcD2E(−). The clones derived from the Saos-2 cells transfected with pcD2E-1Bd or pcD2E(−) were named S(+)1, 2, 3, 4, and 5 or S(−)1, 2, 3, 4, and 5, respectively, and the clones derived from the BT-549 cells transfected with pcD2E-